NASA CR-132264

Buckling Behavior of Composite Cylinders Subjected to Compressive Loading

By R. L. Carri

June 1973

Prepared under contract NAS1-11817 by
GRUMMAN AEROSPACE CORPORATION
Bethpage, New York

for

Langley Research Center
NATIONAL AERONAUTICS AND SPACE ADMINISTRATION

FOREWORD

This report was prepared by Grumman Aerospace Corporation, Bethpage, L.I., New York under contract NAS1-11817, "Buckling Behavior of Composite Cylinders Subjected to Compressive Loading". Analysis and fabrication of specimens was performed at the Grumman Corporation facilities. Instrumentation, testing and comparisons of several analytical buckling theories were performed at the NASA Langley Research Center.

This contract was conducted under the sponsorship of the Materials Application Branch of the Materials Division of the NASA Langley Research Center. Mr. H. Benson Dexter, Composites Section, was the NASA project monitor. The program manager at Grumman was Mr. R.N. Hadcock and the assistant program manager was Mr. S.J. Dastin.

The author wishes to acknowledge the following individuals who have contributed to the program.

Mr. A. Angiola	Structural Design
Mr. R. Collins	Quality Control
Mr. A. DeAngelis	Manufacturing Engineering
Mr. G. Golam	Materials and Processes
Mr. M. Kanal	Structural Analysis
Dr. J. Whiteside	Structural Mechanics

CONTENTS

BUCKLING BEHAVIOR OF COMPOSITE CYLINDERS SUBJECTED TO COMPRESSIVE LOADING

By R.L. Carri

SUMMARY

Room temperature compressive buckling strengths of eight cylinders, four boron-epoxy and four boron-epoxy reinforced-titanium, with diameter to thickness ratios ranging between 40 and 67 are determined experimentally and compared with analytical predictions. Numerical buckling strengths are presented for Donnell's, Flugge's and Sanders' shell theories for anisotropic and orthotropic material cases. Comparison of analytical predictions with experimental results indicates good agreement and the recommended correlation factor suggested in the literature is applicable for design. For the cylinders tested in this investigation the correlation between experiment and theory ranged from 0.73 to 0.97.

INTRODUCTION

In recent years the use of high modulus and low mass composite materials, most notably boron-epoxy, for the fabrication of lightweight tubular compression members has been successfully demonstrated. Initial experimental investigations (Refs. 1 and 2) were based on the compressive strength and column efficiencies of tubular members while recent hardware oriented programs (Refs. 3 and 4) included designing for local buckling modes of failure.

The technology to structurally optimize and analyze a composite tubular compression member for geometrical configuration, filament orientation and stacking sequence has been reasonably defined (Refs. 3, 5 and 6). However, experimental results are lacking for local buckling of composite cylinders particularly for diameter-thickness ratios (D/t) approximately equal to 50. The purpose of this program was to establish a correlation between theoretical and experimental compressive buckling strengths for boron-epoxy composite cylinders and boron-epoxy reinforced-titanium cylinders with D/t's < 70.

Page intentionally left blank

SYMBOLS

The units for physical quantities used in this report are given in both the International System of Units (SI) and the U.S. Customary Units. Measurements and calculations were made in U.S. Customary Units. Conversion factors relating the two systems are given in Reference 7, and those pertinent to this report are presented in Appendix A.

D	mean cylinder diameter, meters (inches)
D_{11}, D_{22}	bending stiffness per unit width of wall in longitudinal and transverse direction, newton-meters (pound-inch)
E_{11}, E_{22}	Young's moduli of orthotropic material in longitudinal and transverse direction, newtons/meter^2 (pounds force/inch^2)
$\bar{E}_{11}, \bar{E}_{22}$	extensional stiffness of wall in longitudinal and transverse direction; $\bar{E}_{11} = \frac{E_{11}t}{(1-\nu_{12}\nu_{21})}$; $\bar{E}_{22} = \frac{E_{22}t}{(1-\nu_{12}\nu_{21})}$, newtons/meter (pounds force/inch)
L	length of cylinder, meters (inches)
l_{tr}	length of transition region near end of cylinder where local bending occurs, meters (inches)
M	bending moment in cylinder wall per unit width of circumference, newton-meters/meter (pound force-inches/inch)
M_o, V_o	bending moment and radial shear force in cylinder wall, at end of cylinder, per unit width of circumference, newton-meters/meter (pound force-inches/inch); newtons/meter (pounds force/inch)
n	number of full waves in cylinder buckle pattern in circumferential direction
$\bar{N}_x$	axial load per unit width of circumference for cylinder subjected to axial compression, newtons/meter (pounds force/inch)

P	compressive axial load, newtons (pounds force)
r	mean cylinder radius, meters (inches)
t	thickness of cylinder wall, meters (inches)
t_R	local thickness of cylinder wall in reinforced region, meters (inches)
x	coordinate in the longitudinal direction of cylinder
Y_i	distance from the neutral axis of the laminate to the ith layer, meters (inches)
γ	correlation factor to account for disparity between analytical and experimental buckling loads
ν_{12}, ν_{21}	major Poisson's ratio and minor Poisson's ratio, respectively

Subscripts

cal	calculated
exp	experimental
i	ith layer of a multilayered composite
max	maximum

MATERIALS AND SPECIMENS

The experimental program consisted of room temperature axial compression testing of eight cylinders, four boron-epoxy composite and four boron-epoxy reinforced-titanium. The specimens were designed to fail in the local buckling mode, and ranged from 38.1 cm (15.0 in.) to 46.4 cm (18.3 in.) in length and had mean diameters ranging from 9.27 cm (3.65 in.) to 9.78 cm (3.85 in.). Details of the cylinders are illustrated in Figures 1 and 2 for the boron-epoxy composite and the boron-epoxy reinforced-titanium specimens, respectively. Local buckling failures in the straight portion of the cylinders were desired, so additional unidirectional plies were added at the ends (Figures 1 and 2) in an attempt to preclude failures due to support and rotational restraints. The specimens were fabricated in two phases. Those with the letter 'a' were fabricated after the first three were tested. The decision to do this was based on incorporating design revisions for the cylinder ends should they be required. Based on the successful Phase 1 test results the end reinforcement concept was considered satisfactory and no revisions were necessary. Table I presents the basic geometry, laminate orientation, and stacking sequence for all of the individual specimens. The boron-epoxy material required for fabrication of all specimens was purchased to existing Grumman specifications in 7.62 cm (3.00 in.) wide tape containing 0.01 mm (0.004 in.) diameter filaments preimpregnated with a 450 K (350°F) stable epoxy resin system.

BORON-EPOXY COMPOSITE SPECIMENS

The approach used to fabricate the all-composite specimens was based on panel processes, so that the tube properties, both mechanical and physical, are similar to those of flat laminates. This was accomplished using a male mandrel upon which the plies of boron-epoxy prepreg and bleeders were convolute wrapped (see Figure 3) and then transferred to a female

mold form prior to curing. The proper number of bleeders and boron-epoxy plies were wound on the mandrel so that the resulting layup was 0.013 cm (0.005 in.) to .051 cm (.020 in.) smaller in diameter than the corresponding inside diameter of the female mold. This tolerance is required to permit proper fitting of the wrapped assembly into the female mold while still providing a fit-up that results in a controlled volume fraction array in the cured cylinder. Figure 4 shows the aluminum male mandrel and the two piece steel female mold form, the inside surface of which is the tool face. A production tube wrapping machine (Figure 5) was used to facilitate the continuous wrapping of all specimens. The wrapping machine consists of a wind-up roller, pressure roller, vacuum table and tube layup mandrel. This continuous wrapping technique utilizes a mylar template, Figure 6, on which individual plies of boron-epoxy are accurately placed prior to wrapping. Information on the template includes the individual ply number, trim, filament orientation, position, slit locations, and template feed rate. To utilize this wrapping technique the mylar template is drawn based on calculating the individual ply developed lengths and includes overlap requirements of .91 cm (.36 in.) for the $\pm$.785 rad ($\pm$45°) angle plies and 1.27 cm (.50 in.) for the 1.57 rad (90°) plies. In addition the 1.57 rad (90°) plies are split longitudinally into two segments, such that the ply is layed up in two halves with one half overlapping the other. This permits the prepreg to expand to the female mold during the cure cycle.

BORON-EPOXY-REINFORCED TITANIUM SPECIMENS

Fabrication of the boron-epoxy reinforced-titanium cylinders consisted of mounting the pretreated and primed titanium substrate on an aluminum mandrel. A single ply of a film adhesive, Metlbond 329 Type 1A, was applied to the titanium followed by the individual boron-epoxy plies, nylon peel ply and spiral wrapped bleeder plies. The tube wrapping machine was used to continuously wrap these specimens also. The bleeder system was tightly overwrapped with plastic shrink tape and the assembly envelope-bagged for curing.

All specimens fabricated for the program were autoclave cured at 450 K (350°F) in accordance with the cure cycles included in Appendices B and C and post-cured in an oven at 463 K (375°F). Photomicrographs of typical cross sections of the fabricated specimens (Figure 7) show the uniformity of the filament spacings which resulted from the fabrication processes used.

TEST METHODS

The eight specimens were tested in axial compression in a 1340-kN (300-kip) capacity hydraulic test machine at the NASA-Langley Research Center Structures and Materials Laboratory. Hardened steel discs were used between the test specimen and the machine platen for load introduction directly into the boron-epoxy composite in bearing. A typical test setup is shown in Figure 8. Instrumentation consisted of foil-type strain gages bonded on the inside and outside surfaces of the specimens and linearly variable differential transformers (LVDT's) which indicated relative motion between the upper and lower platens of the test machine. The location and circuit numbers of the strain gages are shown in Figure 9. All tests were conducted at room temperature at a uniform strain rate of .0038 cm/cm (.0015 in/in) per minute until the specimen failed. Loads, strains and displacements were recorded at a virtually continuous rate in the Langley central digital data recording facility. Prior to testing, each specimen was loaded to 20 percent of its anticipated failing load and the platen of the test machine was aligned to obtain an equal strain readout from four axial strain gages located at mid-length around the outside circumference of the specimen.

TEST RESULTS

Typical data obtained from tests of the eight specimens in the form of load strain curves are presented in Figure 10. The experimental elastic modulus for each specimen was obtained utilizing the linear portion of the

curves corresponding to the strains at mid-length of the specimens. Failure of the specimens occurred at the indicated maximum loads which coincided with the buckling loads for the all-composite specimens, see Figures 10(a) and (b) . The load strain curves for the composite-reinforced titanium specimens indicated a varying degree of strain reversal prior to failure as shown in Figures 10 (c),(d) and (e). The coalescence of buckling and material failures is attributed to the low D/t ratios of the specimens. Load deflection data for all specimens was linear to failure. A typical load deflection plot is shown in Figure 11.

Photographs showing the location and type of failures are presented in Figure 12. Figure 12(a) illustrates local buckling of a typical all-composite specimen and shows the complete composite material failure which was typical of all specimens tested. There were no discernable buckles or indications of failure prior to ultimate collapse. All failures occurred almost instantaneously and were accompanied by a loud noise and a sudden reduction in load. Figure 12(b) shows the failures obtained for the initial three specimens tested during phase one. The shiny surface appearance of the cylinders resulted from a protective epoxy spray coating applied to the first three specimens after fabrication. This coating caused difficulty in strain gage installation and was omitted on the second group of specimens. Figures 12(c) and 12(d) are photographs showing the failures for the second group of specimens. The material failures of the all-composite specimens shown in Figure 12(c) are more pronounced than the failures of the composite-reinforced titanium specimens shown in Figure 12(d). This is even more evident when comparing the end views of the failed composite-reinforced titanium specimens shown in Figure 12(e) with those of the all-composite ones shown in Figure 12(f). The titanium acts to restrict the failure to a localized area where the titanium is buckled.

ANALYSIS

Selection of Specimen Configurations

The specimen geometries presented in Table I were determined by several considerations. A diameter sufficient to facilitate the installation of strain gages on the inside surface of the specimens was required.

Laminate thickness was selected to produce a low D/t ratio such that local stability was critical under axial compressive loading. The all-composite cylinders, 100-11a and 100-13, were optimized by varying the percentages of lamina orientation and the stacking sequence to yield the highest theoretical buckling stress for the 0, $\pm$0.785, 1.57 rad (0°, $\pm$45°, 90°) family of laminates. This was accomplished using the orthotropic non-homogeneous buckling analysis of Reference 5, which is based on small deflection buckling theory and Donnell-type stability equations. Figure 13 shows the results of the optimization study performed for specimen 100-11(a). The maximum compressive strength envelope shown in the figure is the inter-laminar shear cutoff for boron-epoxy which remains relatively constant for laminates having more than 50 percent of 0 rad (0°) filaments.

The configurations of the composite-reinforced titanium specimens are based on three considerations. First, the calculated stress in the titanium substrate at buckling, including the residual stresses resulting from the elevated cure of the composite, must be below 821 MN/m^2 (119.0 ksi), the stress at which the tangent modulus decreases sharply for annealed Ti-6Al-4V (see Figure 14). Second, an overwrap of a pair of angle plies $\pm$0.785 rad ($\pm$45°) is necessary to prevent longitudinal cracks from developing in the composite material due to the transverse residual stresses resulting from the dissimilarities of the constituent material coefficients of thermal expansion and Youngs moduli. The third consideration was to select three arbitrary percentages of boron-epoxy composite reinforcement to verify the selective reinforcement concept for various D/t ratios.

Cylinder Buckling Strengths

The method of analysis initially used to predict the compressive buckling strengths of all specimens was based on Donnell-type stability equations for multi-layered orthotropic cylinders (Ref. 5). Because of the apparently low buckling strengths obtained from the first three specimens tested, it was decided to examine other buckling analysis methods. This investigation was conducted by H. Benson Dexter of the Composites

Section at Langley during the fabrication of Phase II specimens and the results were not obtained in time to incorporate possible changes in the specimen laminate configurations, which had been optimized for Donnell's theory.

The accuracy of Donnell's equations were investigated by Hoff (Ref. 8) for isotropic shells. Hoff shows that Donnell's equations can result in considerable errors for cylinders that buckle with a small number of circumferential waves ($n \leq 4$). Hoff also recommends that Donnell's theory should be replaced by a solution of the Flugge equations when the cylinder is short. Since the Donnell theory indicated buckling mode shapes of ($n \leq 4$) for all specimens tested in this program, it was decided to reanalyze the cylinders using Flugge and the more recent Sanders shell theories.

Numerical results for Flugge's theory were obtained using an iteration scheme to find the critical buckling load. The procedure developed and coded by Wu (Ref. 9) is applicable for general anisotropic cylinders with arbitrary ply orientations. Numerical results for Sanders' theory were obtained using the SALORS (Structural Analysis of Layered Orthotropic Ring-Stiffened Shells) computer program (Ref. 10). This program which uses a finite difference procedure for solution of the buckling problem was developed at the NASA Langley Research Center.

Buckling strengths for all specimens were calculated both for the classical simple support and clamped boundary conditions. The material properties used in the calculations are presented in Table II. A summary of the theories and orthotropic and anisotropic cases for which numerical results were obtained are as follows:

- Flugge:
  - Anisotropic - (Ref. 9)
  - Orthotropic - (Ref. 9)
- Sanders:
  - Orthotropic - (Ref. 10)
- Donnell:
  - Anisotropic - (Ref. 9)
  - Orthotropic - (Ref. 9)
  - Orthotropic - (Ref. 5)

For the anisotropic cases, the material properties for each ply were required input for the computer program. The orthotropic cases required successive $\pm.785$ rad ($\pm 45°$) plies to be lumped as a single layer. All consecutive 0 rad (0°) and 1.57 rad (90°) plies were also lumped as discrete layers of their respective orientations. Analytical results are presented in Table III for the simple support boundary conditions. Results for the clamped boundary conditions were omitted since they differed from the simple support values by less than 5 percent. The specific results presented in Table III show reasonable agreement between Flugge's and Sanders theories with a maximum difference in predicted buckling load of less than 6 percent for specimen 101-11. In contrast, the discrepancies in results between the Flugge and Donnell theories are extreme. The buckling loads computed using the Donnell theory are 12 to 64 percent higher than those predicted using Flugge's theory. In addition the critical circumferential wave numbers for the anisotropic analyses are n = 2 for Flugge's theory in contrast to n = 4, 5 for Donnell's theory. The Donnell theory has been shown to be inaccurate for small n (Ref. 8) and it is apparent from the table of calculated buckling loads that the Donnell theory is not acceptable for any of the specimen configurations. Based on the numerical results the discrepancy between theories increases as the D/t ratio decreases. This was observed both for the all-composite and the composite-reinforced titanium specimens. This can possibly be explained by comparing the assumptions used in the Donnell and Flugge theories. Donnell's assumption for a thin shell is that $t/r \ll 1$ whereas Flugge stipulates $(\frac{t}{r})^3$ is neglibible compared to unity for a thin shell.

The Flugge anisotropic results will be used for comparison with experimental values in later discussion. Since there is reasonable agreement between the numerical results obtained using Flugge and Sanders theories, the former was chosen because of its general familiarity for practical engineering applications.

Correlation Factors

The correlation factor γ is a term used to account for the differences between theoretical buckling analysis and experiment. For isotropic circular cylinders subjected to axial compression the recommended correlation factor (Ref. 11) may be computed by the expression:

$$\gamma = 1 - .901\,(1 - e^{-\phi}) \tag{1}$$

where

$$\phi = \frac{1}{16}\sqrt{r/t} \tag{2}$$

Equation (1) is presented graphically in Figure 15 for isotropic cylinders. For multilayered orthotropic cylinders the correlation factor is of the same form as equation (1) and ϕ is replaced by

$$\phi = \frac{1}{29.8}\left[\frac{r}{4\sqrt{\frac{D_{11}D_{22}}{\bar{E}_{11}\bar{E}_{22}}}}\right]^{1/2} \tag{3}$$

Equation (3) reduces to (2) if the material is considered to be homogeneous. The correlation factors for all specimens were calculated assuming the material to be isotropic, equation (2), and compared to the actual orthotropic nonhomogeneous material case equation (3). The difference between the two cases was less than 2 percent. This is due primarily to the radical in equation (3) which is insensitive to the inhomogeneity of the cylinder wall for the particular laminates studied herein.

End Design for Stability Critical Composite Cylinders Subjected to Axial Compressive Loading

Reinforcement to prevent brooming failures consisted of adding circumferential fiberglass doublers cured on the outside surface of the cylinder and fitting the inside of the specimen with an epoxy potting compound to a depth of 1.3 cm (0.5 in.) on each end. To obtain buckling failures away from the ends of the specimens additional 0 rad (0°) plies of boron-epoxy were added internal to the laminate. These plies are necessary to reduce the local bending stresses which result from the end support and rotational restraints. The required number and length of the reinforcement plies were determined by considering the cylinder to be loaded in axial compression (see Figure 16(a)), with

the ends assumed completely restrained from radial displacement and rotation. The local bending moment resulting from the restraint is rapidly damped out and the length of the transition region, l_{tr}, between the built in edge and the basic cylinder as given by article 11.1 of Reference 12. is

$$l_{tr} \simeq \frac{2\pi}{\beta} \tag{4}$$

where β is the characteristic of the basic cylinder and for orthotropic material was derived to be equal to

$$\beta = \sqrt[4]{\frac{E_{22}t}{4r^2 D_{11}}} \tag{5}$$

To prevent any bending failure in this transition region additional unidirectional boron-epoxy plies are added to the basic laminate to obtain a minimum margin of safety of 15 percent. For preliminary design the maximum required transition thickness t_R was determined using the basic cylinder parameters as follows:

$$\begin{aligned} F_{all} &= f_{membrane} + f_{bending} \\ &= \frac{\bar{N}_x}{t} + \frac{M_o Y_i E_i}{D_{11}} \end{aligned} \tag{6}$$

where F_{all} = Allowable stress in cylinder wall

Y_i = Distance from the neutral axis of the laminate to the i^{th} layer

E_i = Modulus of the i^{th} layer in the longitudinal direction

and $$M_o = \mu_{12} \bar{N}_x \sqrt{\frac{E_{22} D_{11}}{E_{11}^2 t}} \tag{7}$$

(M_o is the maximum bending moment at the assumed built in edge of the cylinder shown in Figure 16(b).)

Substituting equation (7) into (6) and solving for the required transition thickness t_R including a 15 percent margin of safety results in

$$t_R \geq 1.15 \frac{\bar{N}_x}{F_{all}} \left(1 + Y_i \mu_{12} \frac{E_i}{E_{11}} \sqrt{\frac{E_{22} t}{D_{11}}}\right) \tag{8}$$

where F_{all} = 250 ksi for unidirectional boron-epoxy and 119 ksi for Ti-6Al-4V

and

$$\bar{N}_x = Y_{cal} \left(\bar{N}_x\right)_{cal}$$

The required number of unidirectional boron-epoxy reinforcement plies, based on a nominal per ply thickness of 0.0130 cm (.0051 in.) is obtained from

$$\text{No. of plies} = \frac{t_R - t}{.0130}$$

where the units of t_R and t are centimeters.

Having determined the preliminary required thickness for the transition region, the applied load distribution near the ends of the cylinders was calculated using the basic method of analysis presented by Wittrick (Ref. 13). Wittrick presents a solution for the internal shear load and wall bending moment distributions in an isotropic cylindrical tube subjected to internal pressure and a uniform tensile axial load. The cylinder is assumed restrained at the ends. Wittrick's solution was extended to include orthotropic material and shown to be valid for axial compression loads smaller than the classical symmetrical buckling load of the cylinder.

A typical longitudinal bending moment distribution calculated using Wittrick's modified analysis is shown in Figure 17 for specimen 101-13. The two curves shown in the figure were obtained using the basic and the reinforced cylinder parameters. All calculations were performed assuming the cylinder to be continuous, and no attempt was made to couple the basic cylinder laminate with the reinforced ends. The structural integrity of the end reinforcements was checked using the extreme values of bending moment from each curve. For analysis the datum or end of the cylinder was conservatively chosen at the beginning of the fiberglass tab (see Figure 16)

COMPARISON OF TEST DATA WITH ANALYSIS

Experimental and calculated buckling strengths, correlation factors, and elastic moduli are presented in Table IV for all specimens. The agreement between experimental correlation factors and the calculated values is reasonable. A comparison of calculated and experimental correlation factors for all specimens is shown in Figure 18. Six of the eight specimens exceeded the recommended values of the calculated correlation factors. The two specimens which had lower than anticipated experimental loads are 101-11 and 100-11a No. 2. A failure analysis of specimen 101-11 indicated an insufficient number of reinforcement plies were added to the laminate to prevent local end buckling and material failure. The stress in the titanium at the end of the specimen exceeded the compression proportional limit, and initiated the failure. Figure 12(e) shows an end view of the failed specimen with the titanium bearing surface completely rolled over.

A comparison of the calculated and experimental elastic moduli presented in Table IV shows good agreement for all of the specimens with a maximum discrepancy of less than 3 percent.

CONCLUDING REMARKS

Correlation between theoretical and experimental compression buckling loads for boron-epoxy composite and boron-epoxy reinforced titanium cylinders having diameter to thickness ratios between 40 and 70 have been determined. The experimental correlation factors are in good agreement with the correlation factors computed for multilayered orthotropic cylinders from the equations presented in the literature. For the cylinders tested in this investigation the correlation between experiment and theory ranged from 0.73 to 0.97. Calculated buckling strengths were determined using three different shell theories. Buckling strengths predicted with the Donnell theory differed from those predicted using Flugge's and Sanders' shell theories by as much as 64 percent. Buckling failures away from the specimen ends were obtained by locally reinforcing both ends with unidirectional plies of boron-epoxy added internal to the laminate. The longitudinal bending moment distribu-

tion at the ends of the specimens was obtained using a solution proposed by Wittrick, and extended to include orthotropic materials. Based on the experimental results, the analysis was shown to applicable for end design of composite cylinders subjected to compressive loading.

APPENDIX A

CONVERSION OF U.S. CUSTOMARY UNITS TO SI UNITS

The International System of Units (SI) was adopted by the Eleventh General Conference on Weights and Measures, Paris, October 1960, in Resolution No. 12. (See ref. 7.) Conversion factors for the units used herein are given in the following tables:

Physical Quantity	U.S. Customary Unit	Conversion Factor (*)	SI Unit
Angle	Degrees	1.745×10^{-2}	Radians (rad)
Bending Moment	kip-in.	1.130×10^{2}	Newton-Meters (N-m)
Area	in^2	6.452×10^{-4}	Square Meters (m^2)
Force	kip = 1000 lbf	4.448×10^{3}	Newtons (N)
Length	in.	2.54×10^{-2}	Meters (m)
Moduli and Stress	ksi = $kips/in^2$	6.895×10^{6}	Newtons Per Square Meter (N/m^2)
Temperature	(°F + 459.67)	5/9	Degrees Kelvin (K)
Unit Loading	lb/in	1.751×10^{2}	Newtons Per Meter (N/m)

* Multiply value given in U.S. Customary Unit by conversion factor to obtain equivalent value in SI Unit.

Prefixes to indicate multiple of units are as follows:

Prefix	Multiple
milli (m)	10^{-3}
centi (c)	10^{-2}
kilo (k)	10^{3}
giga (G)	10^{9}

APPENDIX B

CURE CYCLE FOR BORON-EPOXY-COMPOSITE CYLINDERS

1. Place part in autoclave and draw 20 inch vacuum minimum.
2. Using CO_2, apply 0.62-0.66 GN/m^2 (90-95 psi) pressure.
3. Check vacuum system, turn vacuum off and measure fall off. If system does not maintain 34 kN/m^2 (10 inches of Hg) after 60 sec. (1 minute), open door and replace hoses and check bag.
4. After system passes leakage test reduce vacuum to 6.8 kN/m^2 (2 inches of Hg) and heat tube to 339-356 K (150-180°F) at 0.62-0.66 GN/m^2 (90-95 psi) pressure.
5. Hold system pressure, temperature, and vacuum of step 4 for 1.8-2.7k sec. (30-45 minutes).
6. Heat part from 339-356 K (150-180°F) to 444-456 K (340-360°F) in 1.8-2.7k sec. (30-45 minutes).
7. At 381 K (225°F), drop pressure to 0.48 ± 0.04 kN/m^2 (70 ± 5 psi).
8. Hold 450 ± 6 K ($350° \pm 10$°F), 0.48 ± 0.04 kN/m^2 (70 ± 5 psi), and 6.8 kN/m^2 (2 inches of Hg) for 5.4 ± 0.3k sec. (90 ± 5 minutes).
9. Cool to 325-333 K (125-140°F) in not less than 2.7k sec. (45 minutes).
10. Apply full vacuum, release pressure and remove from autoclave.
11. Post cure in air circulating oven at $464 \, {}^{+5}_{-0}$ K ($375 \, {}^{+10}_{-0}$°F) for 10.8 ± 0.6k sec. (180 ± 10 minutes) after removing all bleeders. Heat up time to $464 \, {}^{+5}_{-0}$ K ($375 \, {}^{+10}_{-0}$°F) is that of oven set at 464-469 K (375-385°F).

APPENDIX C

CURE CYCLE FOR BORON-EPOXY-COMPOSITE-REINFORCED TITANIUM CYLINDERS

1. After bagging, cover assembly with asbestos.
2. Apply 68 kN/m^2 (20 inches of Hg) vacuum (minimum) and install part in autoclave.
3. Heat laminate to a temperature of 339 $\pm$ 17 K (150 $\pm$ 30°F) while maintaining 68 kN/m^2 (20 inches of Hg).
4. Pressurize to .34 $\pm$ .04 kN/m^2 (50 $\pm$ 5 psi) with CO_2.
5. Check bag for leaks. Turn vacuum system off. If part does not maintain .34 kN/m^2 (10 inches of Hg) vacuum after 60 sec (1 minute), check bag and vacuum system.
6. Vent bag to atmosphere using CO_2, reducing vacuum to a maximum of 6.8 kN/m^2 (2 inches of Hg).
7. Heat laminate to 444 $^{+6}_{-0}$ K (340 $^{+10}_{-0}$°F) within 1.6-2.4k sec. (40-60 minutes).
8. Maintain laminate at a temperature of 444 $^{+6}_{-0}$ K (340 $^{+10}_{-0}$°F) and a pressure of .34 $\pm$ .04 kN/m^2 (50 $\pm$ 5 psi) for 5.4 $\pm$ 0.3 k sec. (90 $\pm$ 5 minutes).
9. Cool to 356 K (180°F) in not less than 2.4k sec. (40 minutes). Draw 68 kN/m^2 (20 inches of Hg) before releasing autoclave pressure. Remove laminate from autoclave.
10. Post cure in air circulating oven at 464 $^{+5}_{-0}$ K (375 $^{+10}_{-0}$°F) for 10.8 $\pm$ 0.6k sec. (180 $\pm$ 10 minutes) after removing all bleeders. Suspend vertically with thermocouples on part as applicable. Heat-up time to temperature is that of oven set at 464-469 K (375-385°F).

Page Intentionally Left Blank

REFERENCES

1. Zender, George W.; and Dexter, H. Benson: Compressive Properties and Column Efficiency of Metals Reinforced on the Surface With Bonded Filaments. NASA TN D-4878, 1968.

2. Dexter, H. Benson: Compressive and Column Strengths of Aluminum Tubing With Various Amounts of Unidirectional Boron/Epoxy Reinforcement. NASA TN D-5938, 1970.

3. Corvelli, Nicholas; and Carri, Robert: Evaluation of Boron-Epoxy-Reinforced Titanium Tubular Truss for Application to a Space Shuttle Booster Thrust Structure. NASA TN D-6778, 1972.

4. Sicari, J. et al.: Fabrication of 1/3 Scale Boron/Epoxy Booster Thrust Structure. Phase I Final Report, Prepared by Grumman Aerospace Corporation for NASA Marshall Space Flight Center under NASA Contract No. NAS8-26675, Sept. 1971.

5. Card, Michael F.: Experiments to Determine the Strength of Filament-Wound Cylinders Loaded in Axial Compression. NASA TN D-3522, 1966.

6. Dow, Norris F.; and Rosen, B. Walter: Structural Efficiency of Orthotropic Cylindrical Shells Subjected to Axial Compression. AIAA J. Vol. 4, No. 3, Mar. 1966, pp. 481-485.

7. Comm. on Metric Pract.: ASTM Metric Practice Guide. NBS Handbook 102, U.S. Dep. Com., Mar. 10, 1967.

8. Hoff, N.J.: The Accuracy of Donnell's Equations. J. Appl. Mech., Vol. 22, Sept. 1955.

9. Wu, C.H.: Buckling of Anisotropic Circular Cylindrical Shells. Ph. D. Thesis, Dept. of Solid Mech. Structures and Mech. Design, Case Western Reserve University, June 1971.

10. Anderson, M.S.; Fulton, R.E.; Heard, W.L. Jr. and Walz, J.E.: Stress, Buckling, and Vibration Analysis of Shells of Revolution. Computers and Structures, Vol. 1, pp. 157-192. Pergamon Press 1971. Printed in Great Britain.

11. Anon.: Buckling of Thin-Walled Circular Cylinders. NASA SP-8007, 1965. (Revised 1968.)

12. Timoshenko, Stephen P.; and Gere, James M.: Theory of Elastic Stability. Second ed., McGraw-Hill Book Co., C. 1961.

13. Wittrick, W.H., Interaction Between Membrane and Edge Stresses for Thin Cylinders Under Axially Symmetric Loading. R.A.S.J., Vol. 67, Mar. 1963.

TABLE I. - SPECIMEN CONFIGURATIONS AND DIMENSIONS

Specimen	Configuration	L		D		D/t	Volume % Boron/Epoxy
		cm	in.	cm	in.		
100-11a No.1	$[\pm 45, 0_5, 90 \pm 45, 90, 0_5, \pm 45]_T$	46.43	18.28	9.27	3.65	39.8	100
-11a No.2		46.43	18.28	9.27	3.65	39.8	100
100-13	$[\pm 45, 0_4, 90_2, 0_4, \pm 45]_T$	42.67	16.80	9.32	3.67	51.4	100
-13a		42.67	16.80	9.32	3.67	51.4	100
101-11	$[\pm 45, 0_{13}, .026\ Ti]_T$	38.10	15.00	9.78	3.85	37.6	75.3
-11a	$[\pm 45, 0_7, .026\ Ti]_T$	38.10	15.00	9.70	3.82	52.1	64.3
101-13	$[\pm 45, 0_4, .026\ Ti]_T$	38.10	15.00	9.73	3.80	67.3	54.6
-13a		38.10	15.00	9.73	3.80	67.3	54.6

TABLE II. - ROOM-TEMPERATURE MATERIAL PROPERTIES

Property	Rigidite 5505 Boron-Epoxy Single - Ply Properties		
	0 rad (0°)	1.57 rad (90°)	±0.785 rad (±45°)
Longitudinal Compression Modulus, GN/m^2 (ksi)	221 (32000)	20 (2900)	18 (2660)
Transverse Modulus, GN/m^2 (ksi)	20 (2900)	221 (32000)	18 (2660)
Shear Modulus, GN/m^2 (ksi)	5 (720)	5 (720)	58 (8420)
Major Poisson's Ratio	0.250	0.0226	0.855
Minor Poisson's Ratio	0.0226	0.250	0.855
Average Layer Thickness, cm (in)	0.0132 (0.0051)		
	Titanium 6Al-4V Annealed		
Youngs Modulus, GN/m^2 (ksi)	110 (16000)		
Shear Modulus, GN/m^2 (ksi)	42 (6150)		
Compression Proportional Limit, MN/m^2 (ksi)	821 (119)		

TABLE III. - COMPARISON OF NUMERICAL COMPRESSIVE BUCKLING SOLUTIONS AND CIRCUMFERENTIAL WAVE NUMBERS

Specimen	Theory, Critical Buckling Loads ($\bar{N}_x$) and Wave Number (n)																	
	Flugge						Sanders			Donnell								
	Anisotropic (Ref. 9)			Orthotropic (Ref. 9)			Orthotropic (Ref. 10)			Anisotropic (Ref. 9)			Orthotropic (Ref. 9)			Orthotropic (Ref. 5)		
	kN/m	lbs/in	n	kN/m	lbs/in	n	kN/m	lbs/in	n	kN/m	lbs/in	n	kN/m	lbs/in	n	kN/m	lbs/in	n
100-11a	3290	18785	2	3291	18792	2	3393	19375	2	5389	30776	4	5205	29725	4	5218	29799	4
100-13	2099	11988	2	2100	11991	2	2170	12393	2	3020	17244	4	3238	18488	4	3135	17902	4
101-11	5002	28565	2	5003	28568	2	5291	30215	2	6212	35472	4	6056	34583	4	5869	33516	3
101-11a	2842	16230	2	2843	16232	2	2945	16815	2	3210	18328	4	3380	19303	2	3275	18703	3
101-13	1926	10996	2	1926	10998	2	1981	11315	2	2152	12288	5	2179	12445	3	2175	12423	0

TABLE IV. - EXPERIMENTAL AND CALCULATED RESULTS FOR LOCAL BUCKLING TEST SPECIMENS

Specimen	t		$(\bar{N}_x)_{exp}$		$(\bar{N}_x)_{cal}$ [a]		$\gamma_{exp} = (\bar{N}_x)_{exp}/(\bar{N}_x)_{cal}$	γ_{cal}	$(E_{11})_{cal}$		$(E_{11})_{exp}$	
	cm	in.	kN/m	lbs/in	kN/M	lbs/in			GN/m^2	ksi	GN/m^2	ksi
100-11a No. 1	.2332	.0918	2593	14805	3290	18785	.79	.77	139	20210	138	20060
-11a No. 2	.2332	.0918	2455	14019	3290	18785	.75	.77	139	20210	140	20250
100-13	.1814	.0714	1753	10008	2099	11988	.83	.75	143	20680	147	21260
-13a	.1814	.0714	2026	11571	2099	11988	.97	.75	143	20680	143	20690
101-11	.2604	.1025	3640	20784	5002	28565	.73	.79	174	25300	176	25490
-11a	.1826	.0719	2236	12770	2842	16230	.79	.75	155	22430	157	22700
101-13	.1438	.0566	1557	8892	1926	10996	.81	.72	137	19830	140	20260
-13a	.1438	.0566	1459	8331	1926	10996	.76	.72	137	19830	138	20000

[a] Flugge's theory anisotropic case Table III

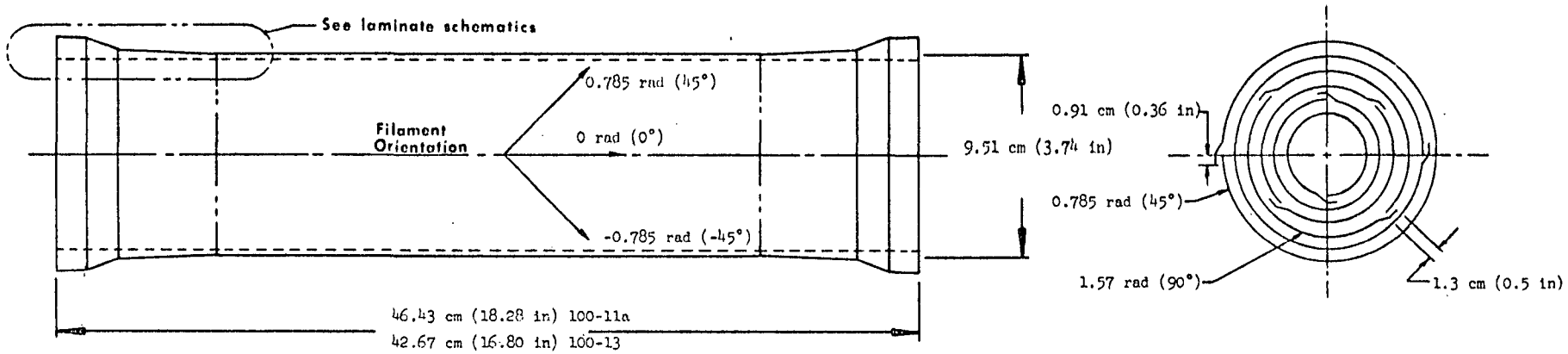

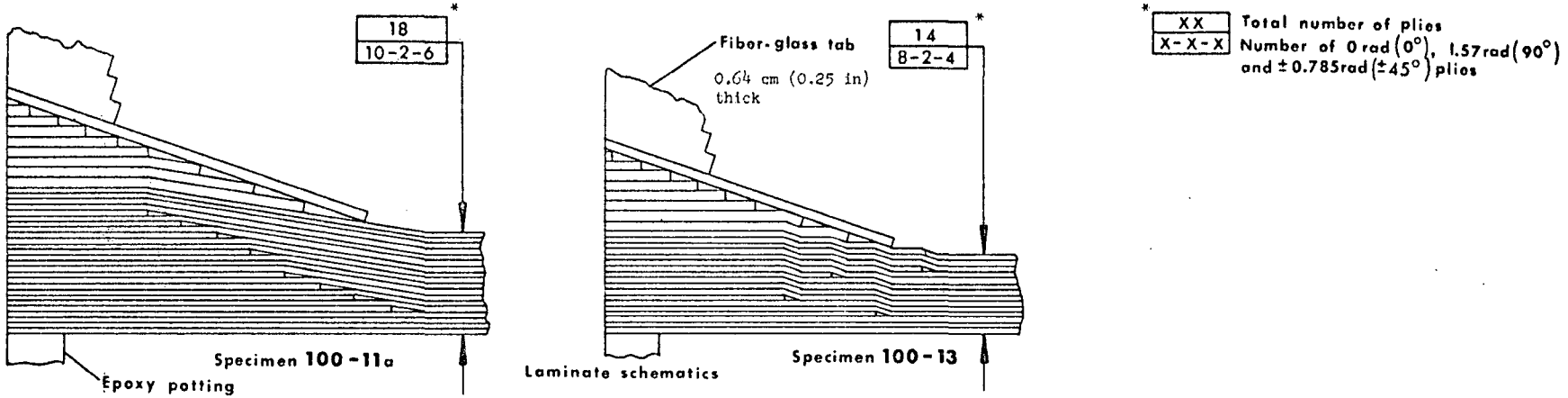

Figure 1.- Boron–epoxy composite specimens

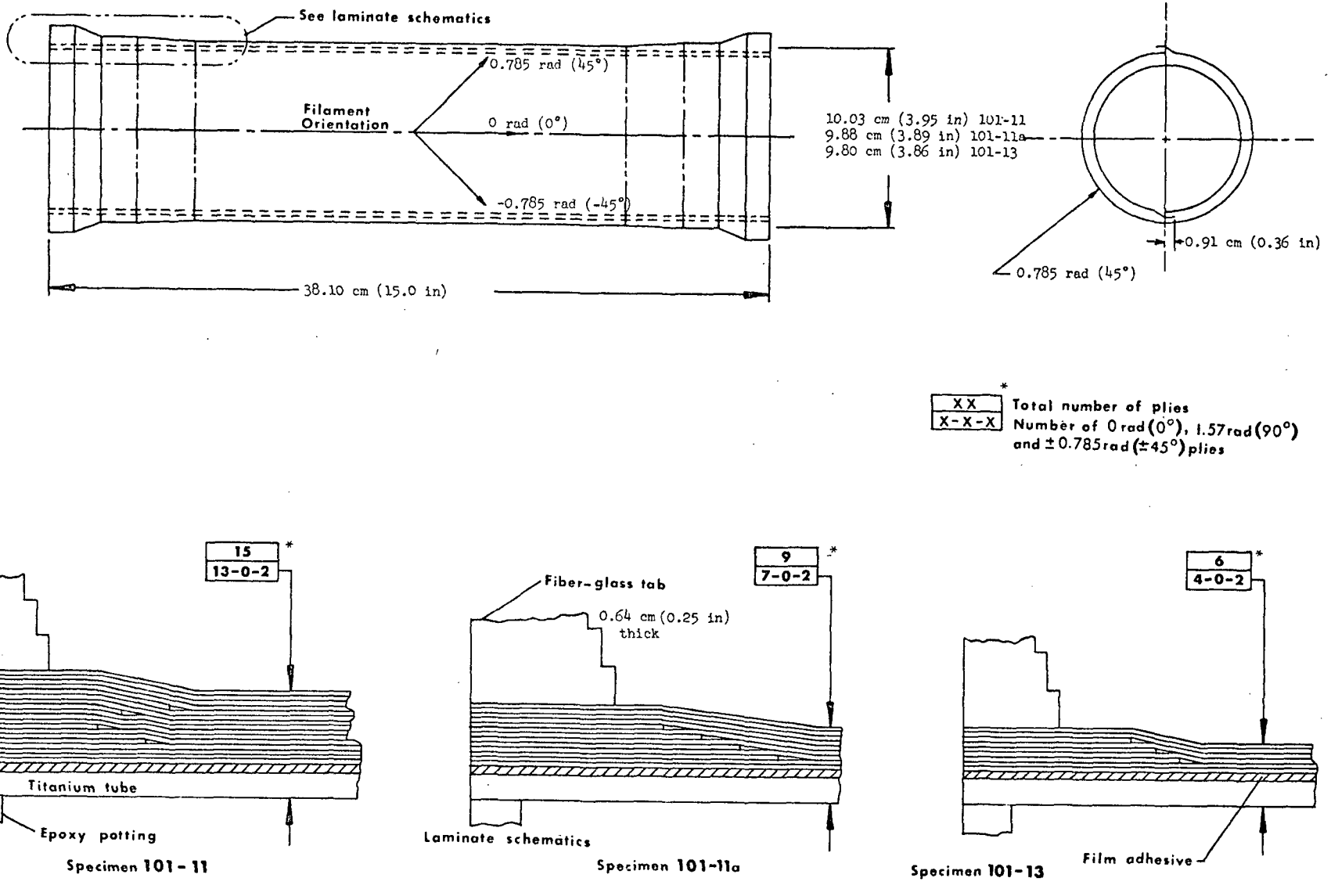

Figure 2.– Boron-epoxy-reinforced-titanium specimens

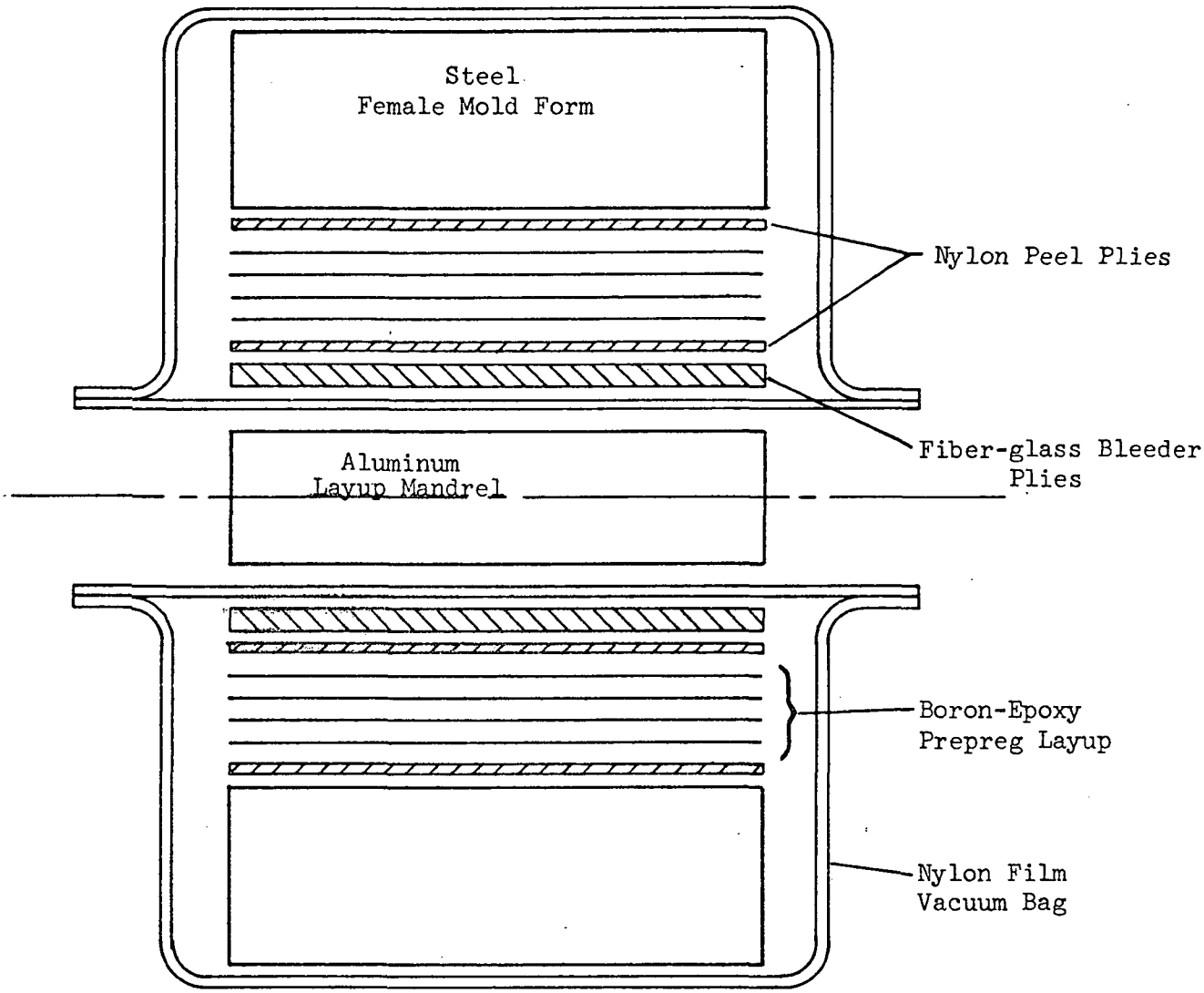

Figure 3. - Cross Section of Layup for All-Composite Cylinders

"Page missing from available version"

pgs. 29-30

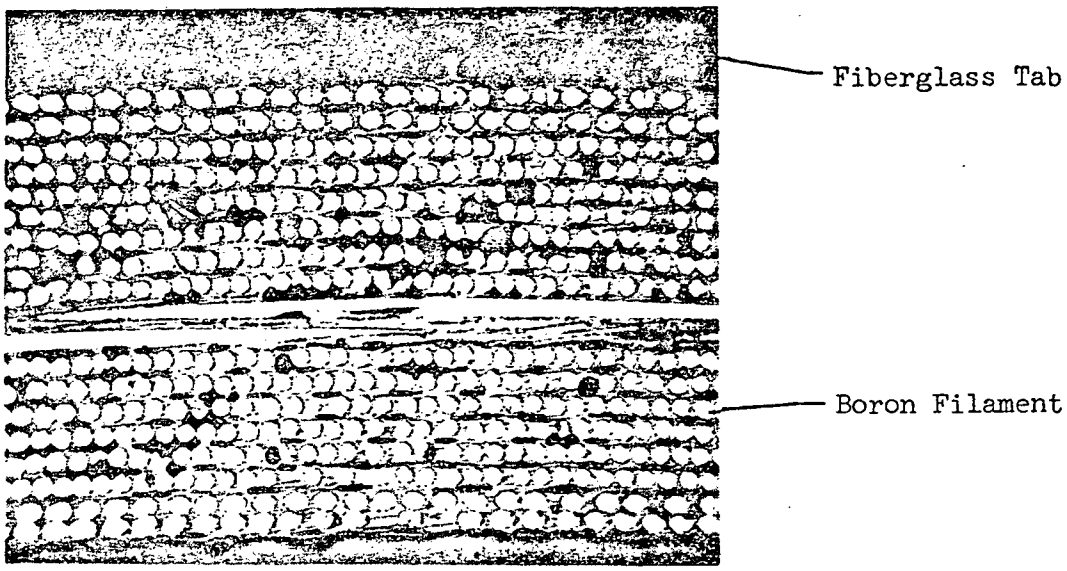

(a) End of Specimen 100-13

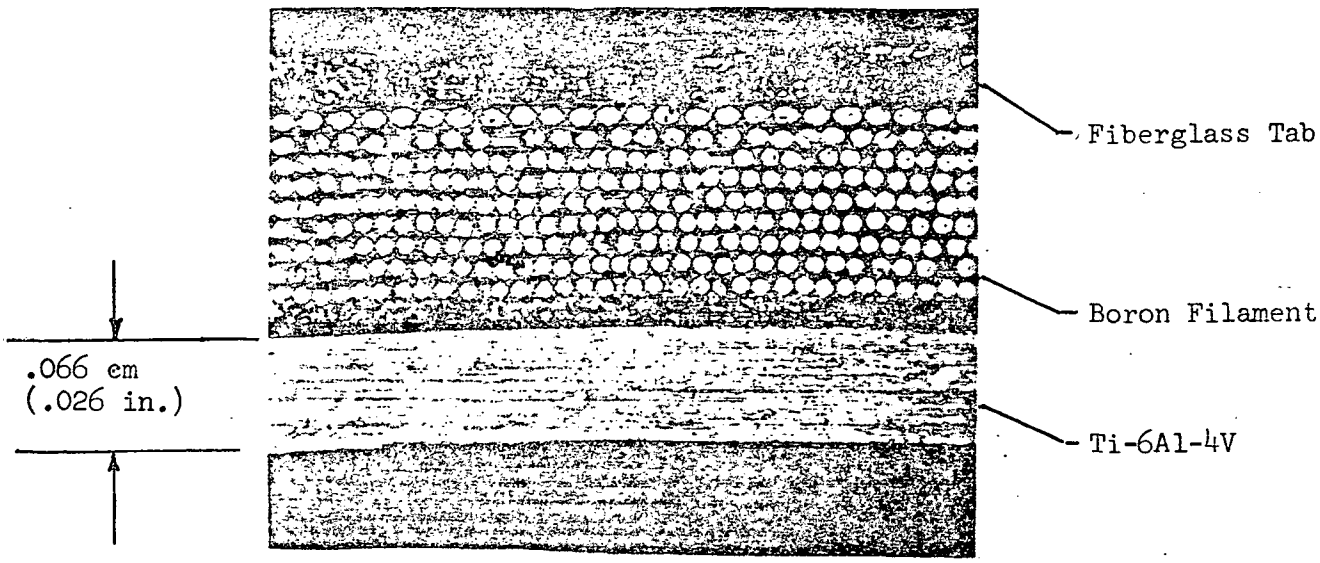

(b) End of Specimen 101-13

Figure 7. Photomicrographs of Typical Specimen Cross-Sections
Magnification 25X

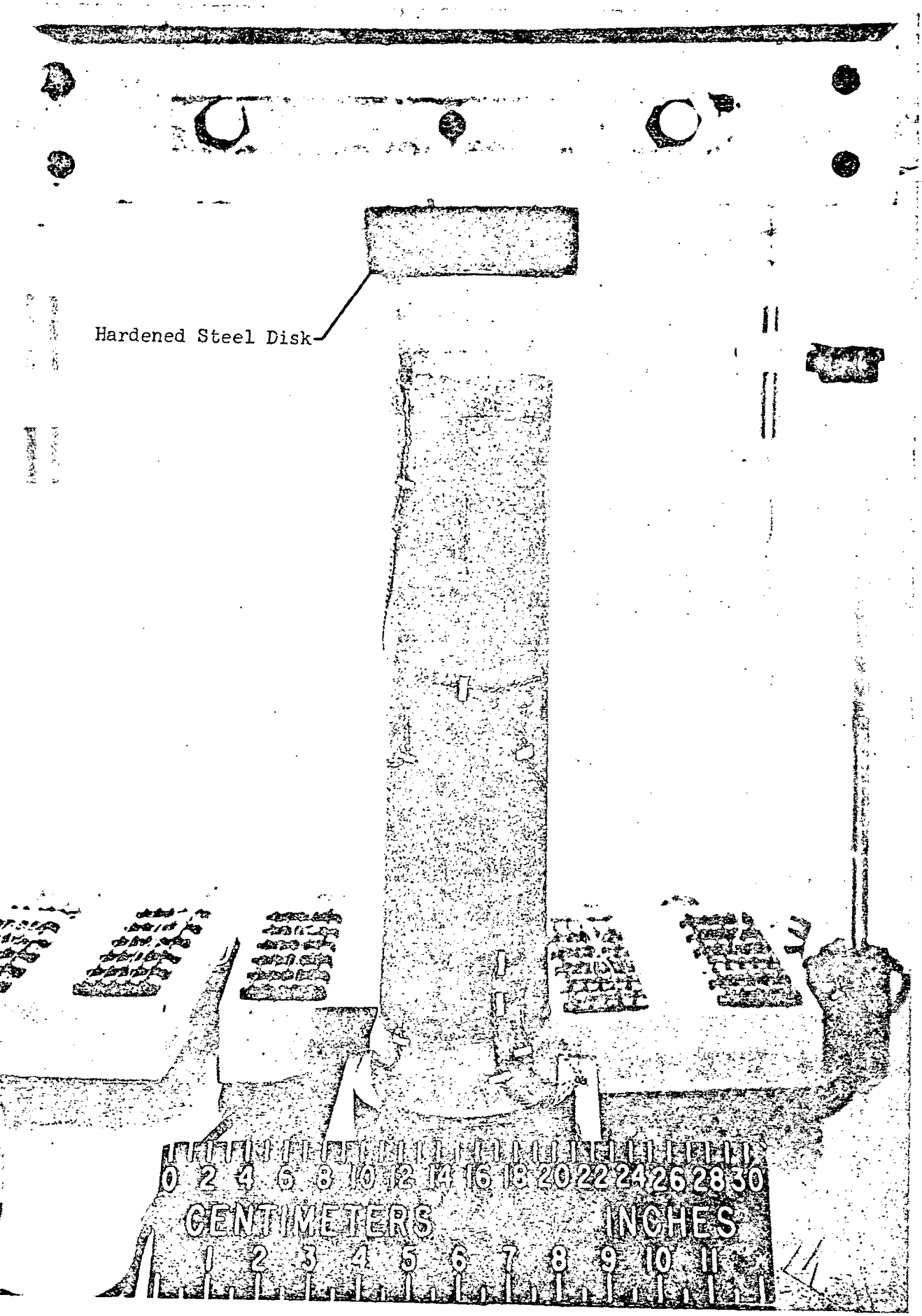

Figure 8. - Compression Test Setup

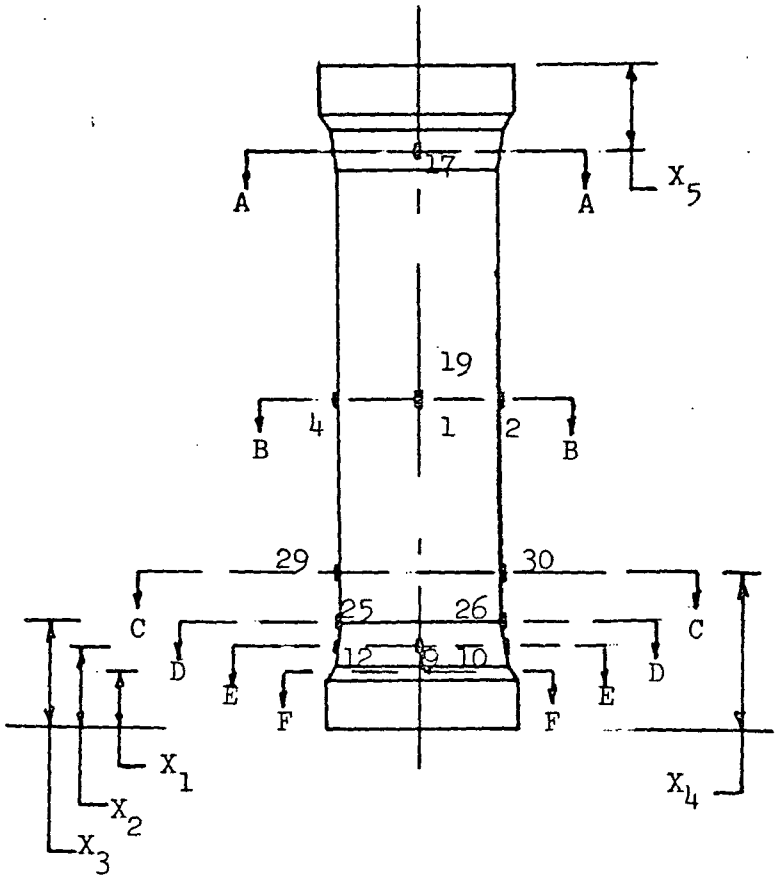

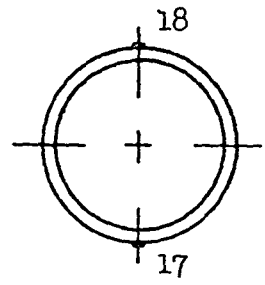

Sect. A-A

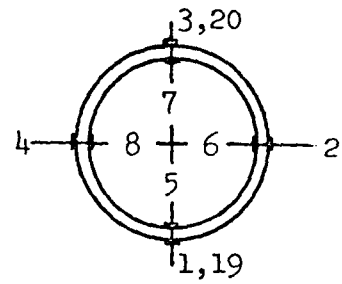

Sect. B-B

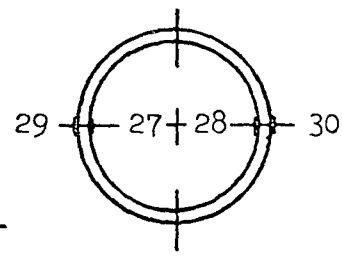

Sect. C-C

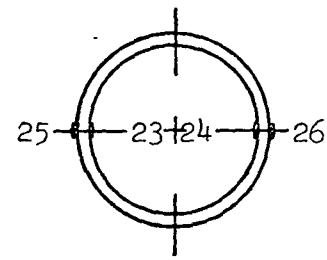

Sect. D-D

NOTE: All gages are axial except 19 and 20 which measure transverse strains

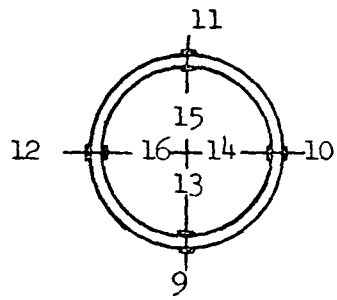

Sect. E-E

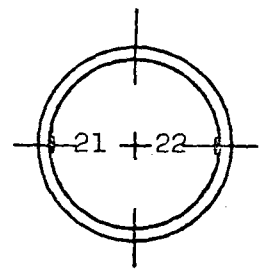

Sect. F-F

Specimen	Dimension									
	X_1		X_2		X_3		X_4		X_5	
	cm	in	cm	in	cm	in	cm	in	cm	in
100-11a	3.81	1.50	5.59	2.20	6.99	2.75	10.16	4.00	5.59	2.20
100-13	----	----	3.30	1.30	----	----	-----	----	3.30	1.30
100-13a	2.54	1.00	3.81	1.50	6.10	2.40	8.38	3.30	3.81	1.50
101-11	----	----	3.30	1.30	----	----	-----	----	3.30	1.30
101-11a	2.54	1.00	4.06	1.60	6.35	2.50	8.64	3.40	4.06	1.60
101-13	----	----	3.30	1.30	----	----	----	----	3.30	1.30
101-13a	2.54	1.00	3.81	1.50	5.84	2.30	7.62	3.00	3.81	1.50

Figure 9. - Location and Identification of Strain Gages

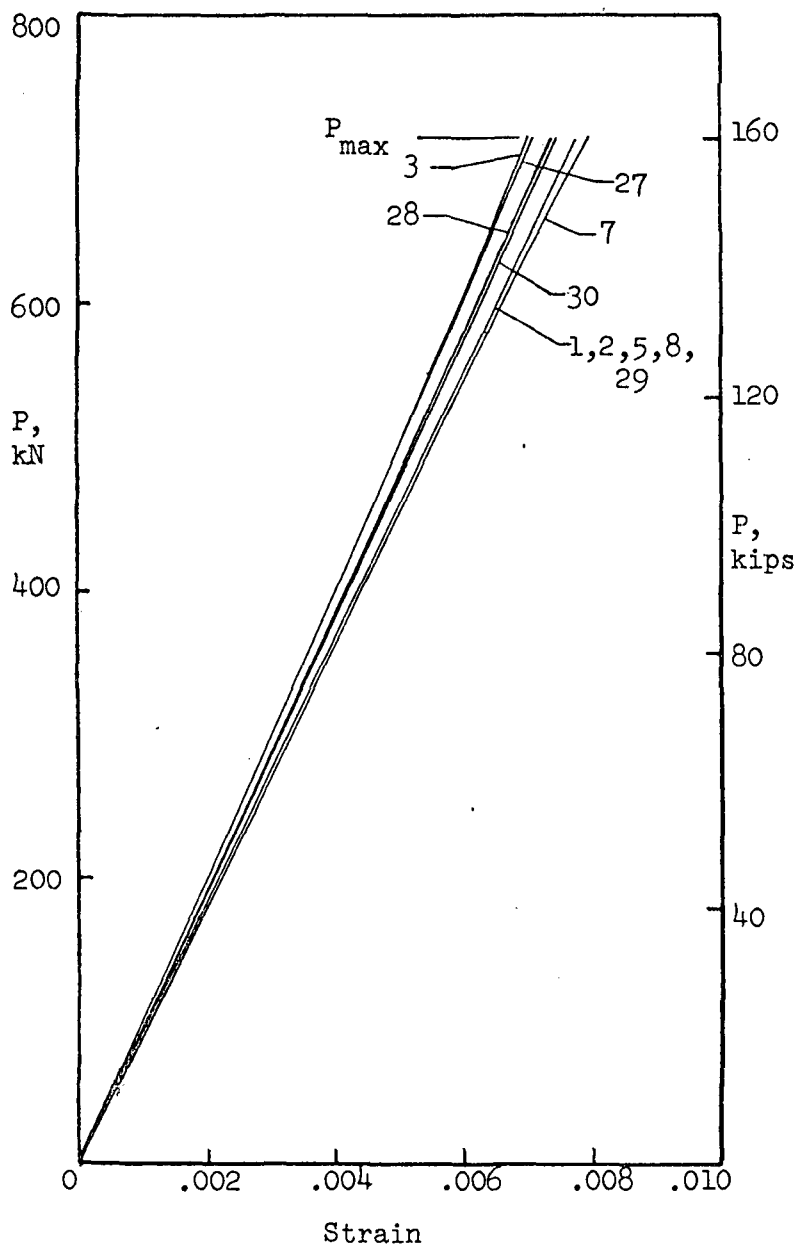

(a) Specimen 100-11a No. 2

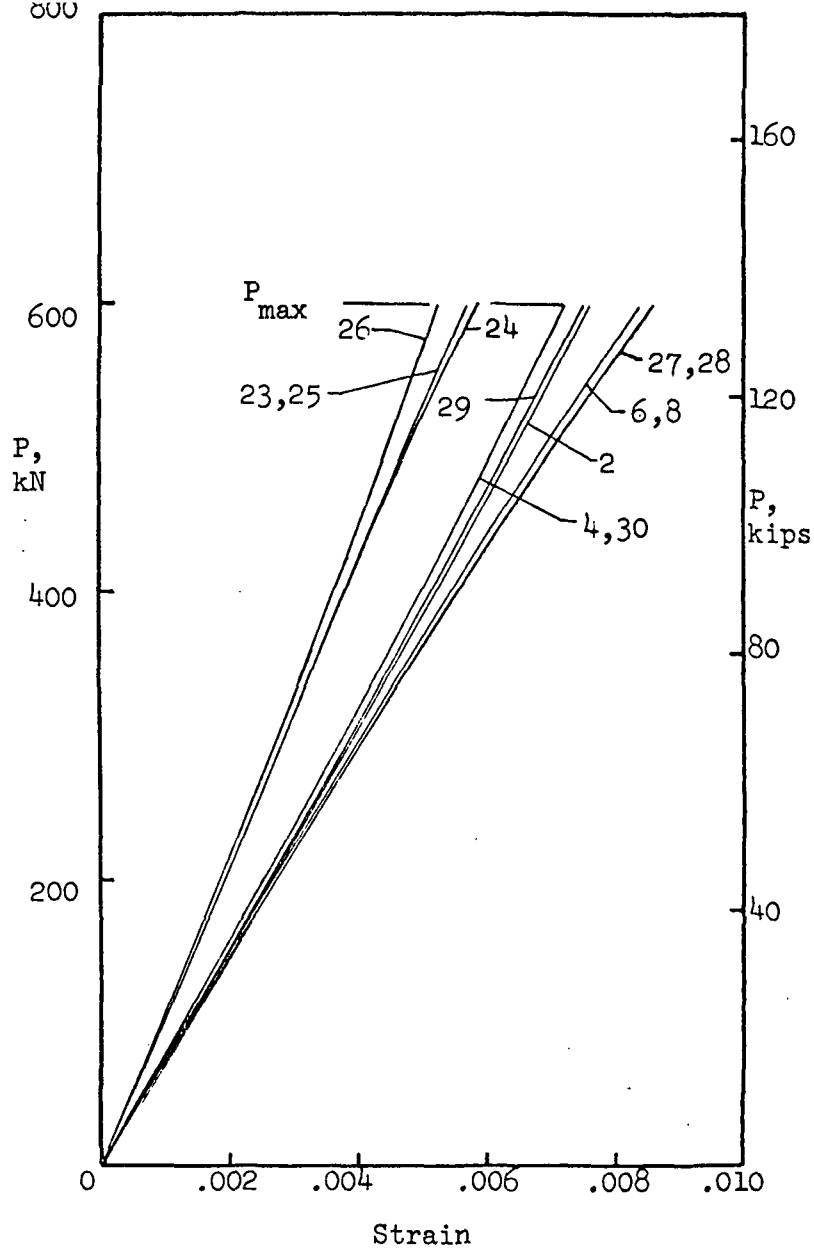

(b) Specimen 100-13a

Figure 10. - Typical Load-Strain Curves From Compression Tests of Specimens at Room Temperature. Numbers Refer to Strain Gage Locations Shown in Figure 9.

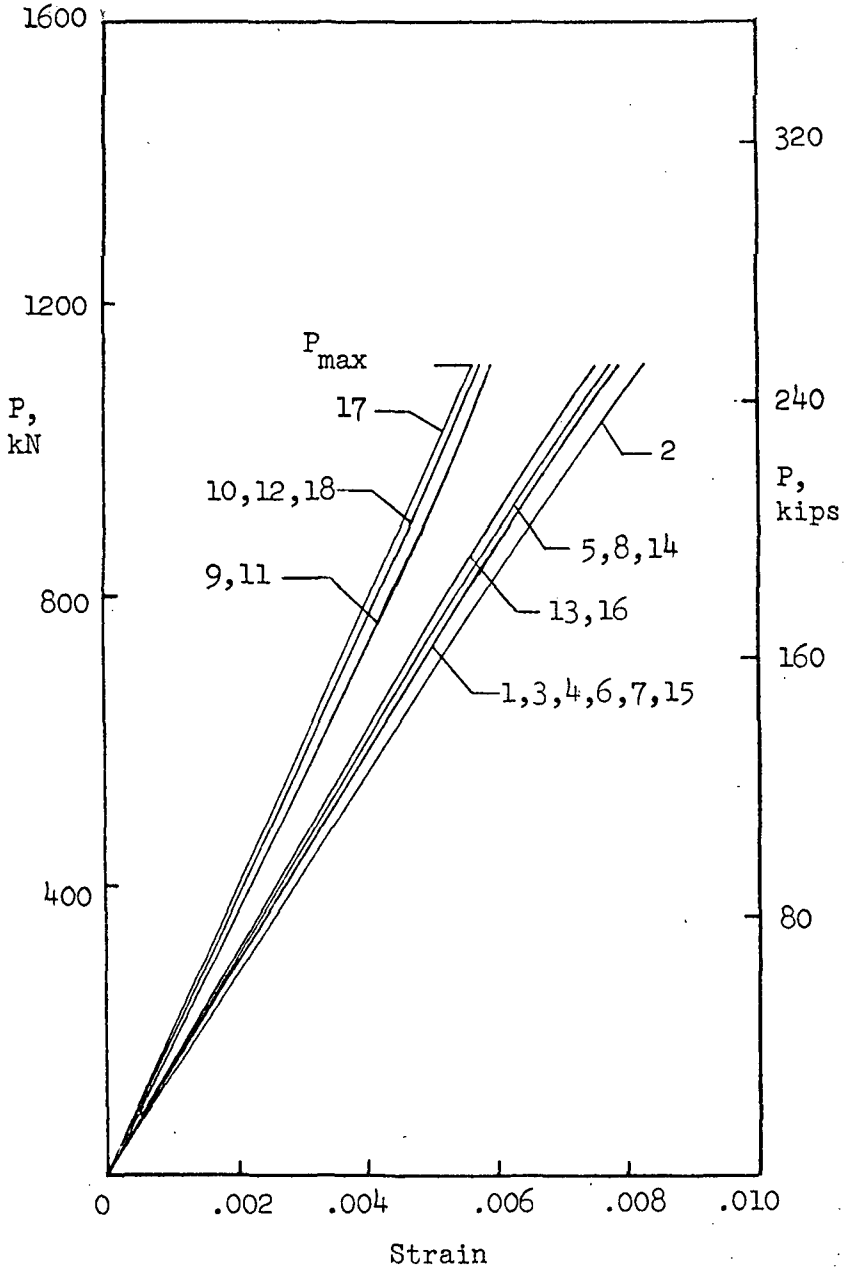

(c) Specimen 101-11

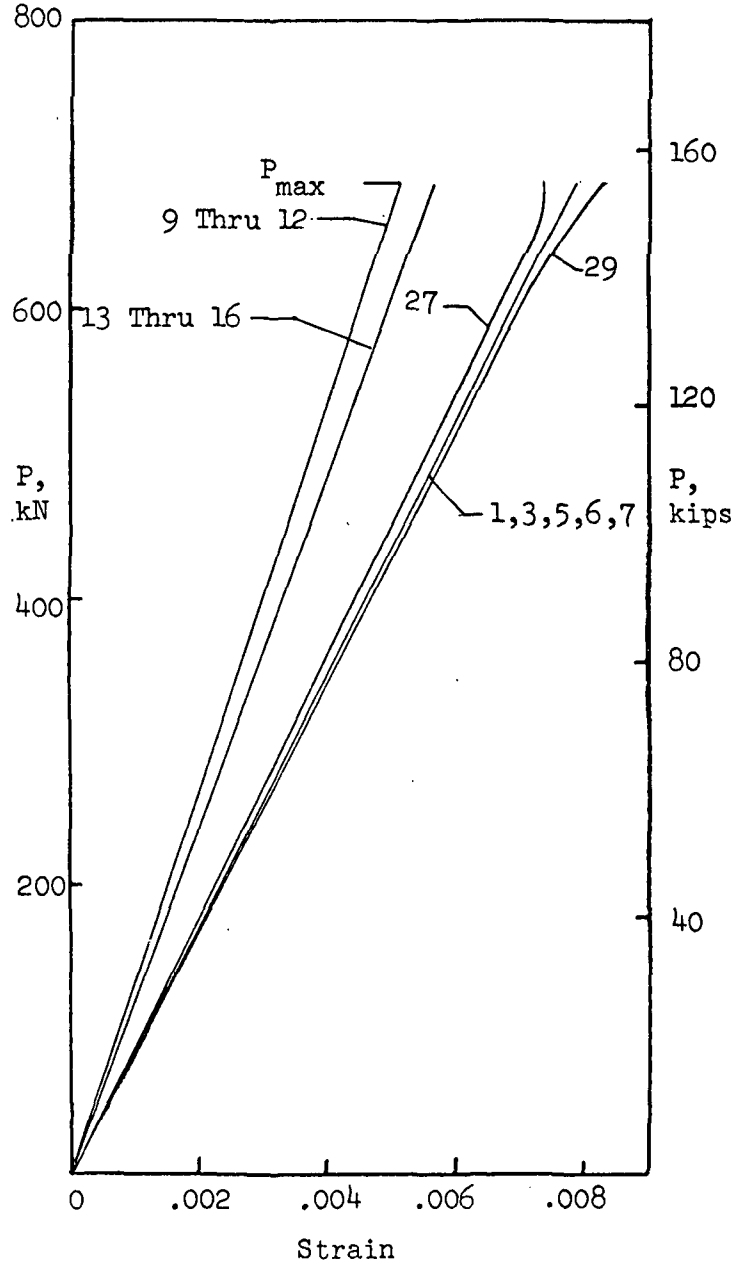

(d) Specimen 101-11a

Figure 10. - Continued

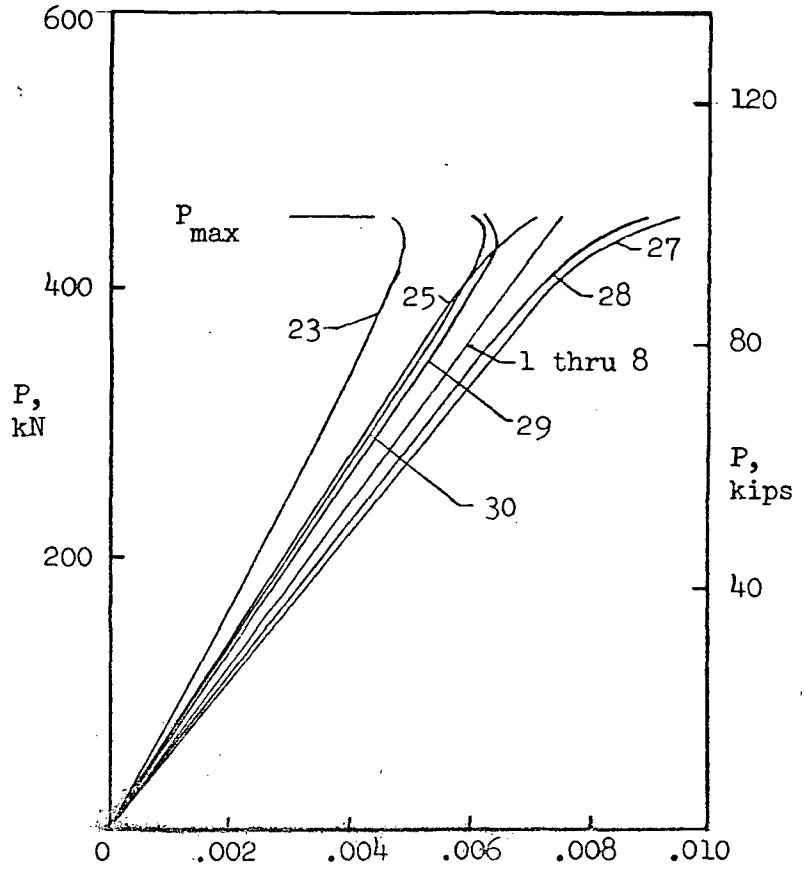

(e) Specimen 101-13a

Figure 10. - Concluded

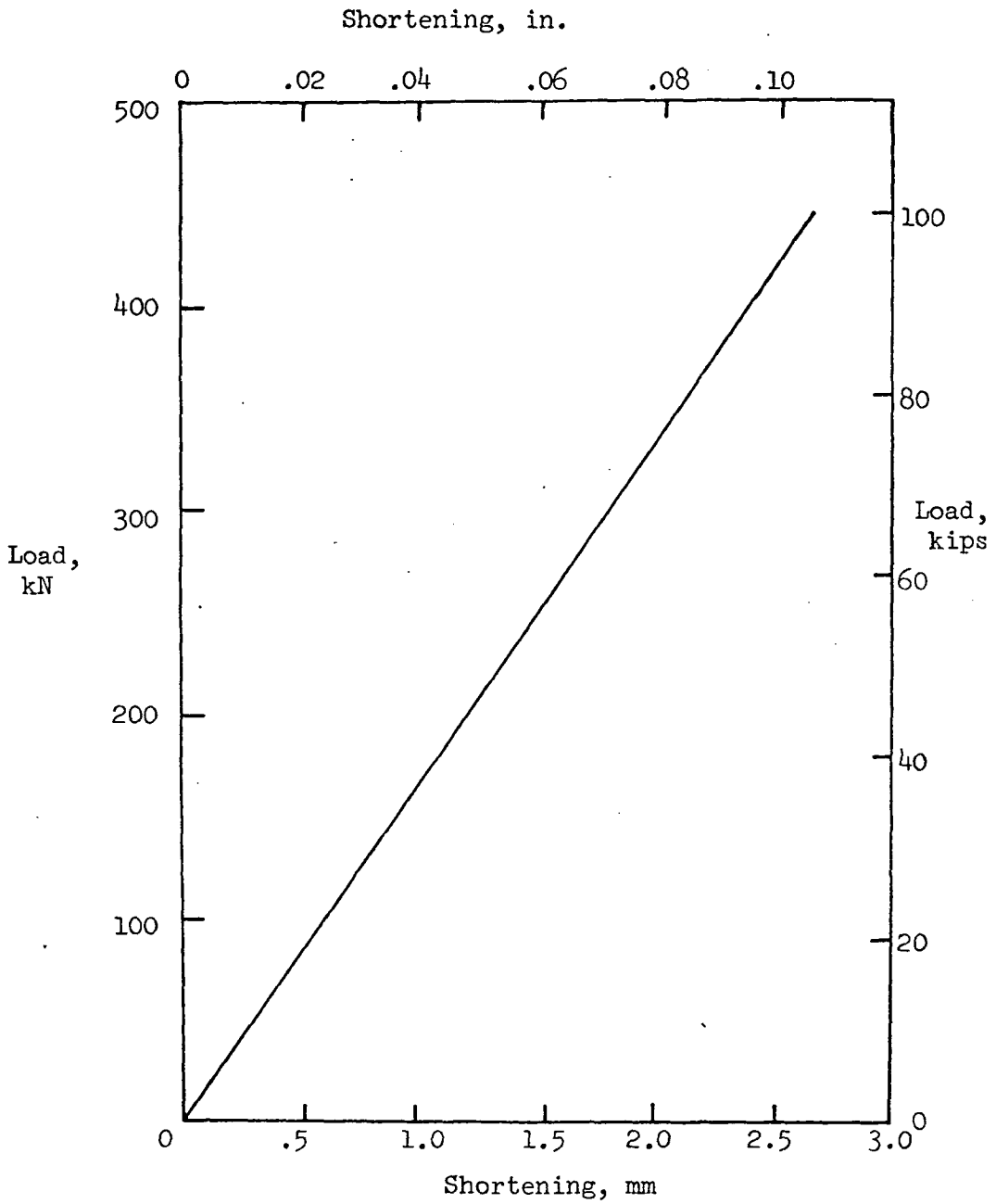

Figure 11. - Load-Shortening Curve For Specimen 101-13a

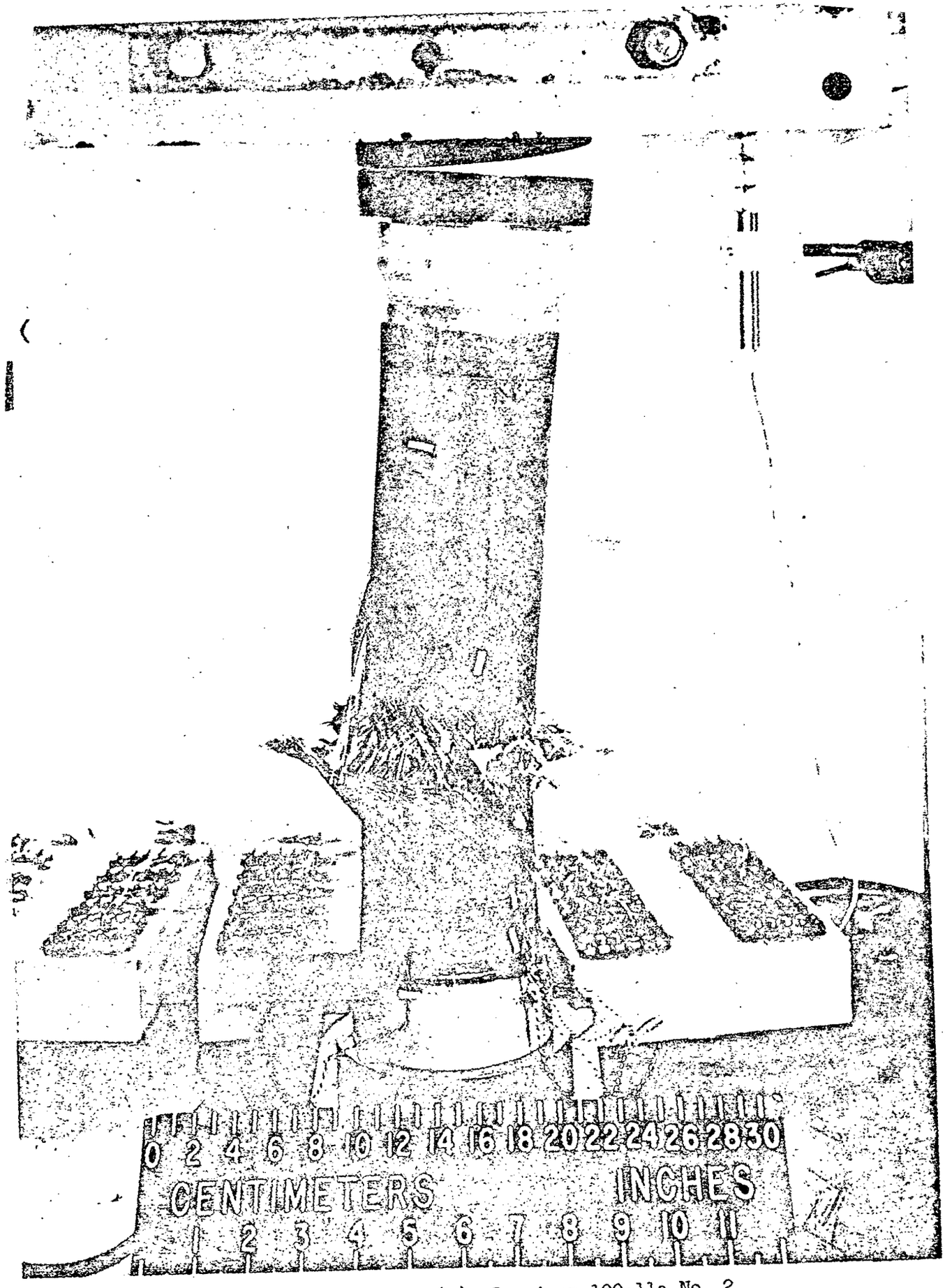

(a) Specimen 100-11a No. 2

Figure 12. - Typical Local Buckling Failures

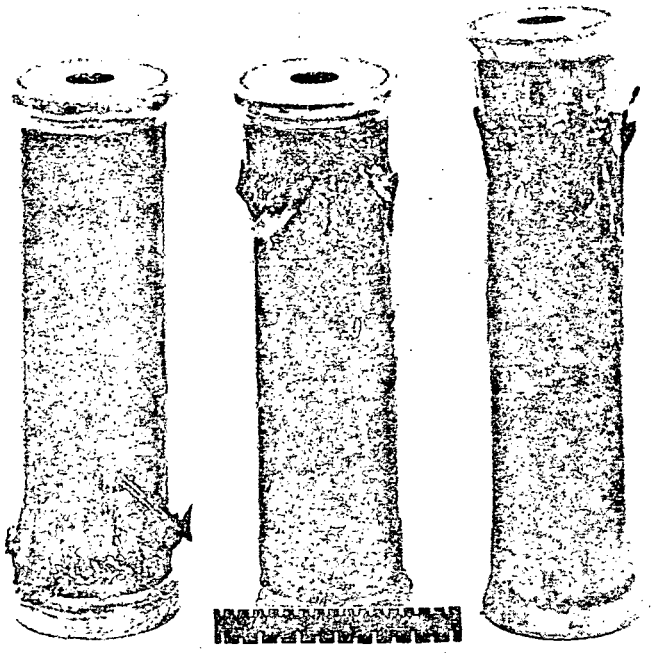

(b) Specimens 101-11 101-13 100-13

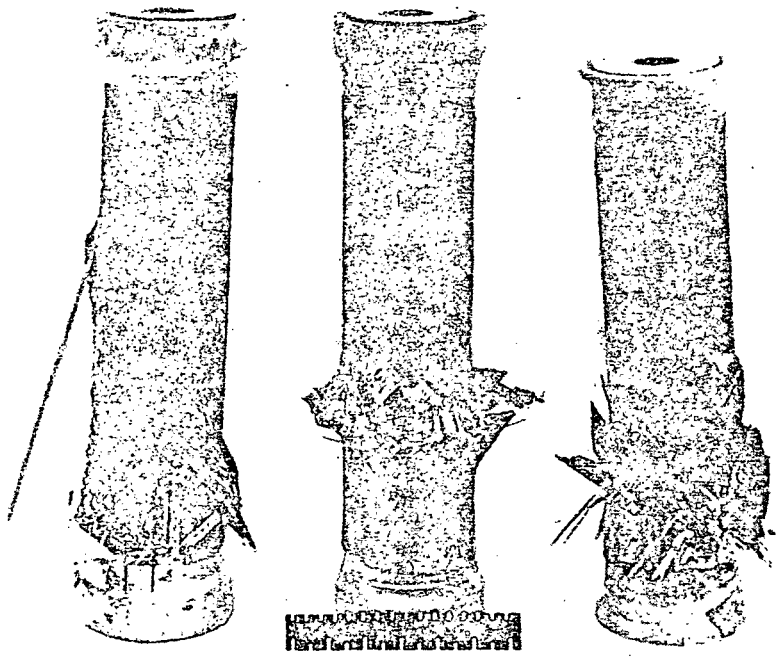

(c) Specimens 100-11a No. 1 100-11a No. 2 100-13a

Figure 12. - Continued

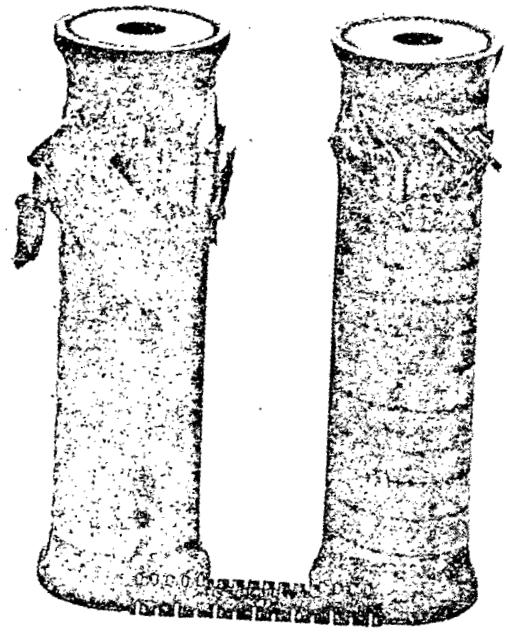

(d) Specimens 101-11a 101-13a

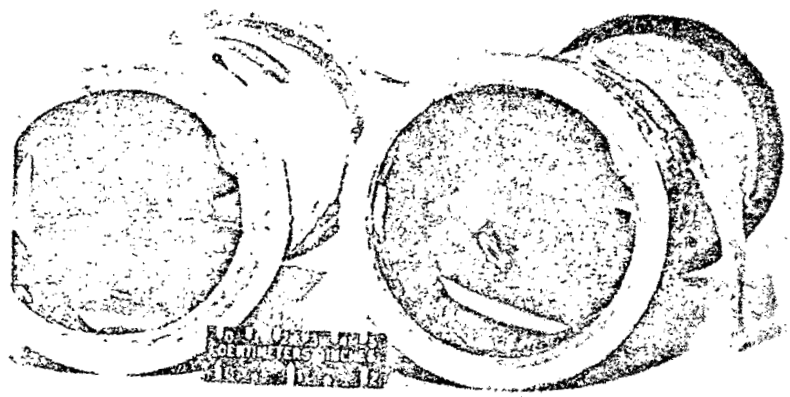

(e) Specimens 101-11 101-11a

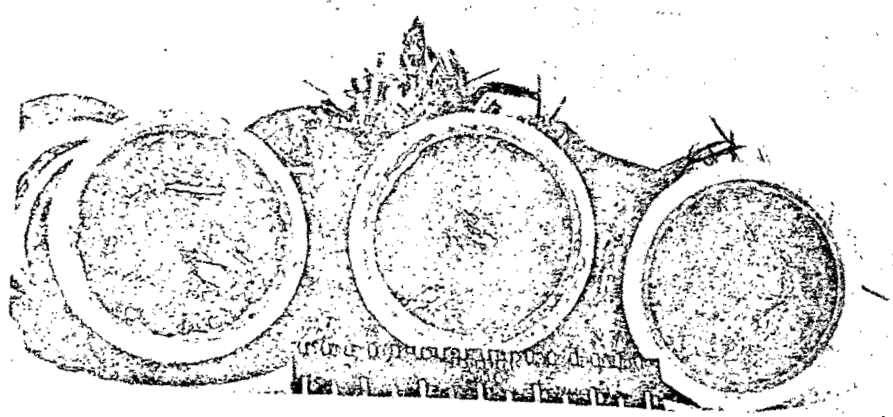

(f) Specimens 100-13 100-11a No. 2 100-13a

Figure 12. - Concluded

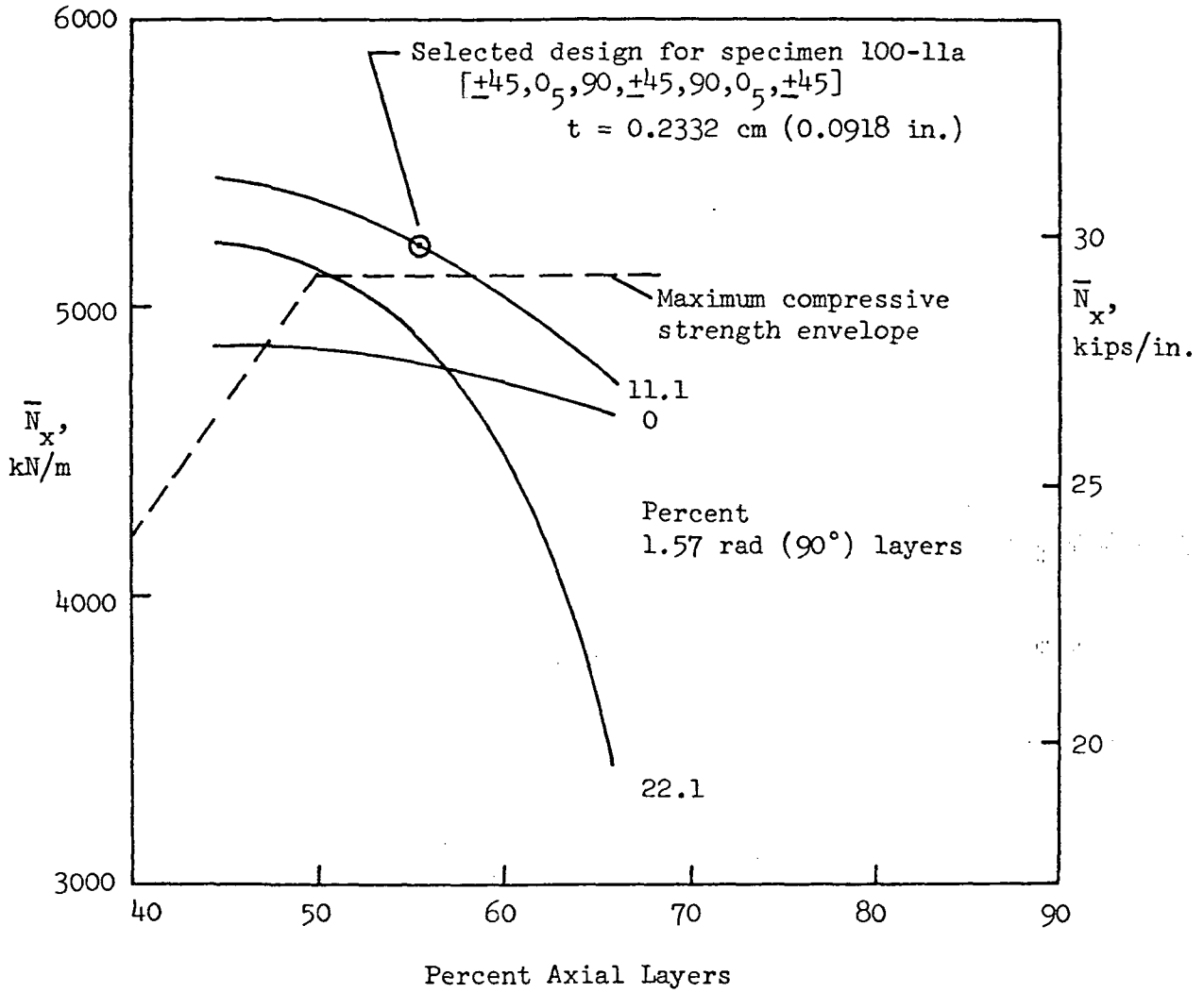

Figure 13. - Laminate Optimization Study

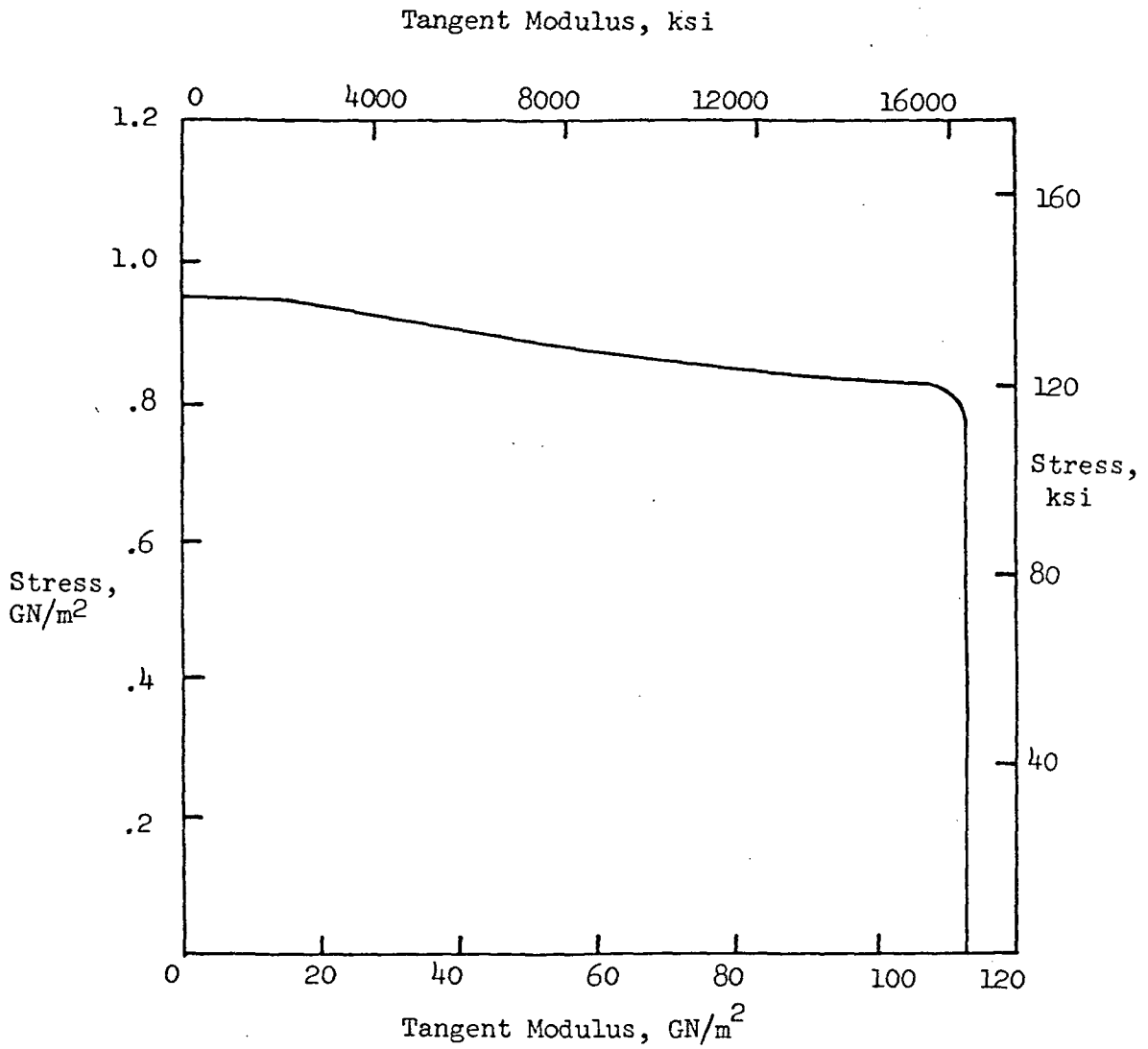

Figure 14. - Compressive Tangent Modulus For Annealed Ti 6Al-4V Alloy Sheet at Room Temperature

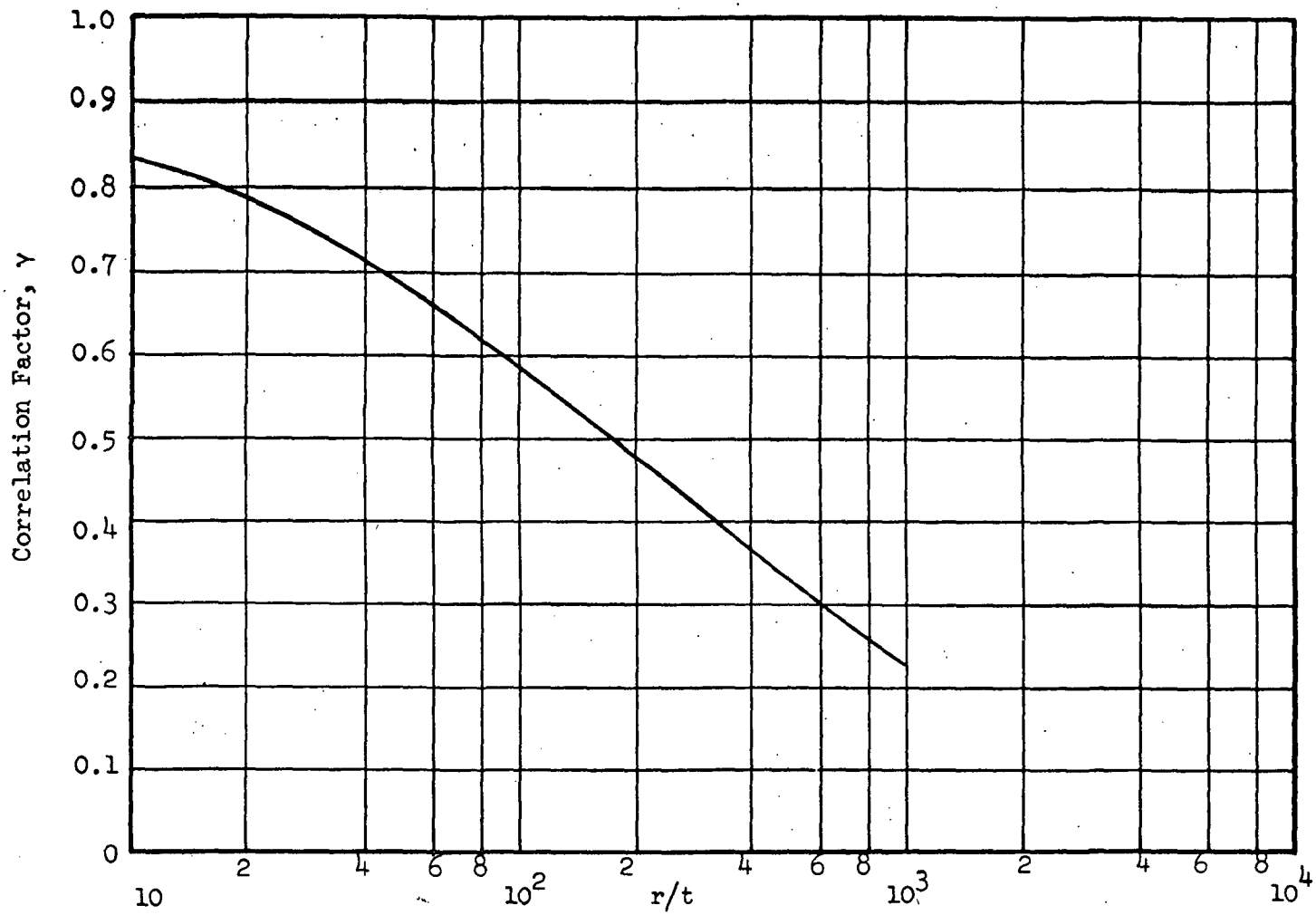

Figure 15. - Correlation Factors for Isotropic Circular Cylinders Subjected to Axial Compression

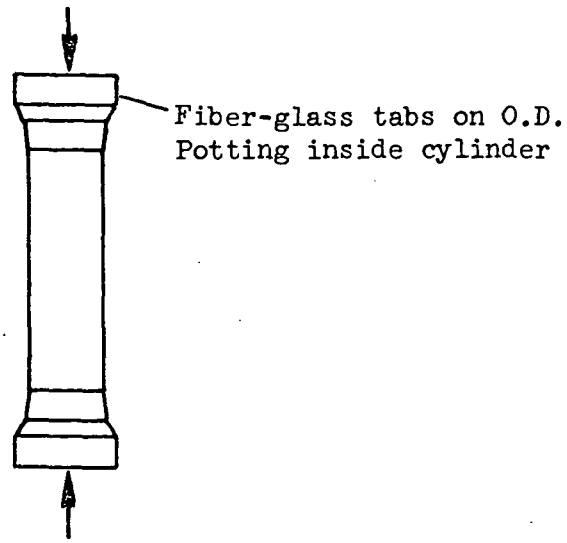

(a) Loading

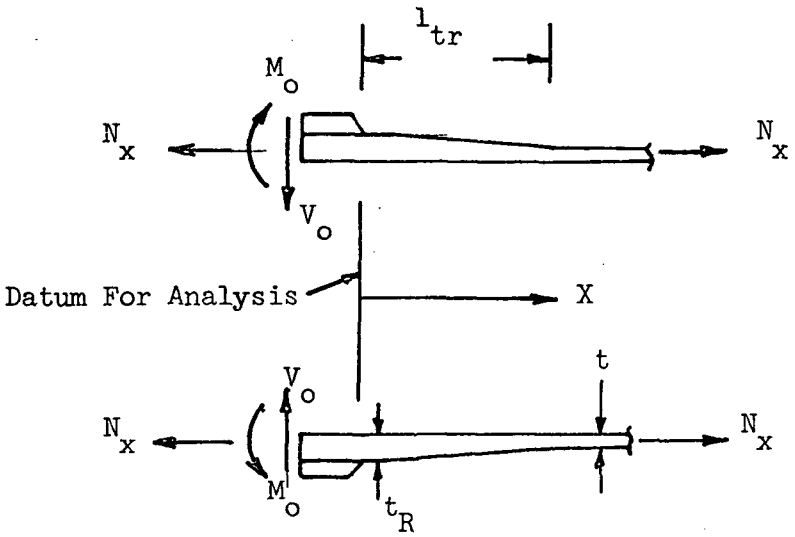

(b) Applied end loads and sign convention

Figure 16. - Cylinder Loading and Applied End Loads

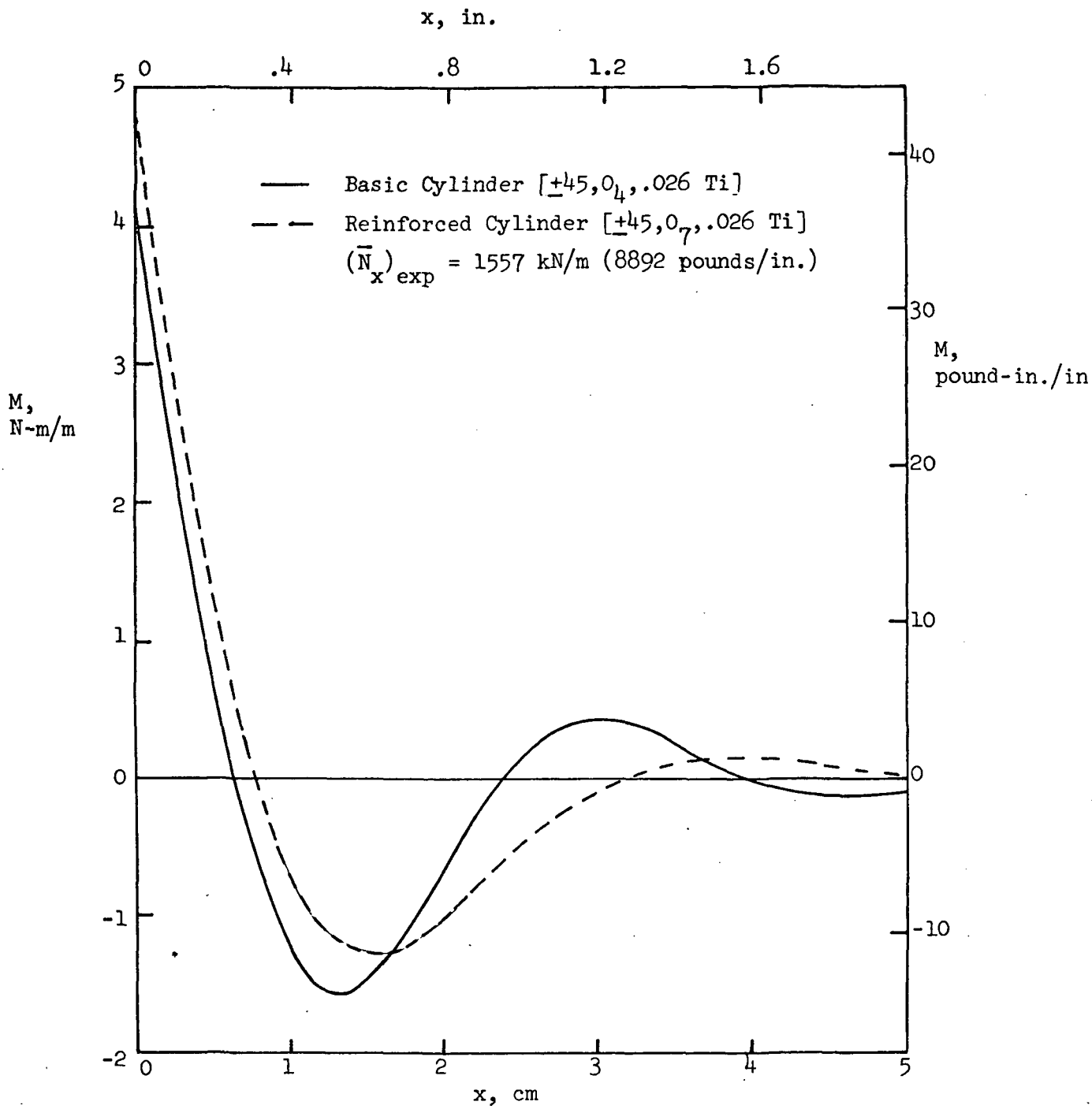

Figure 17. - Calculated Longitudinal Bending Moment in Cylinder Wall for Specimen 101-13

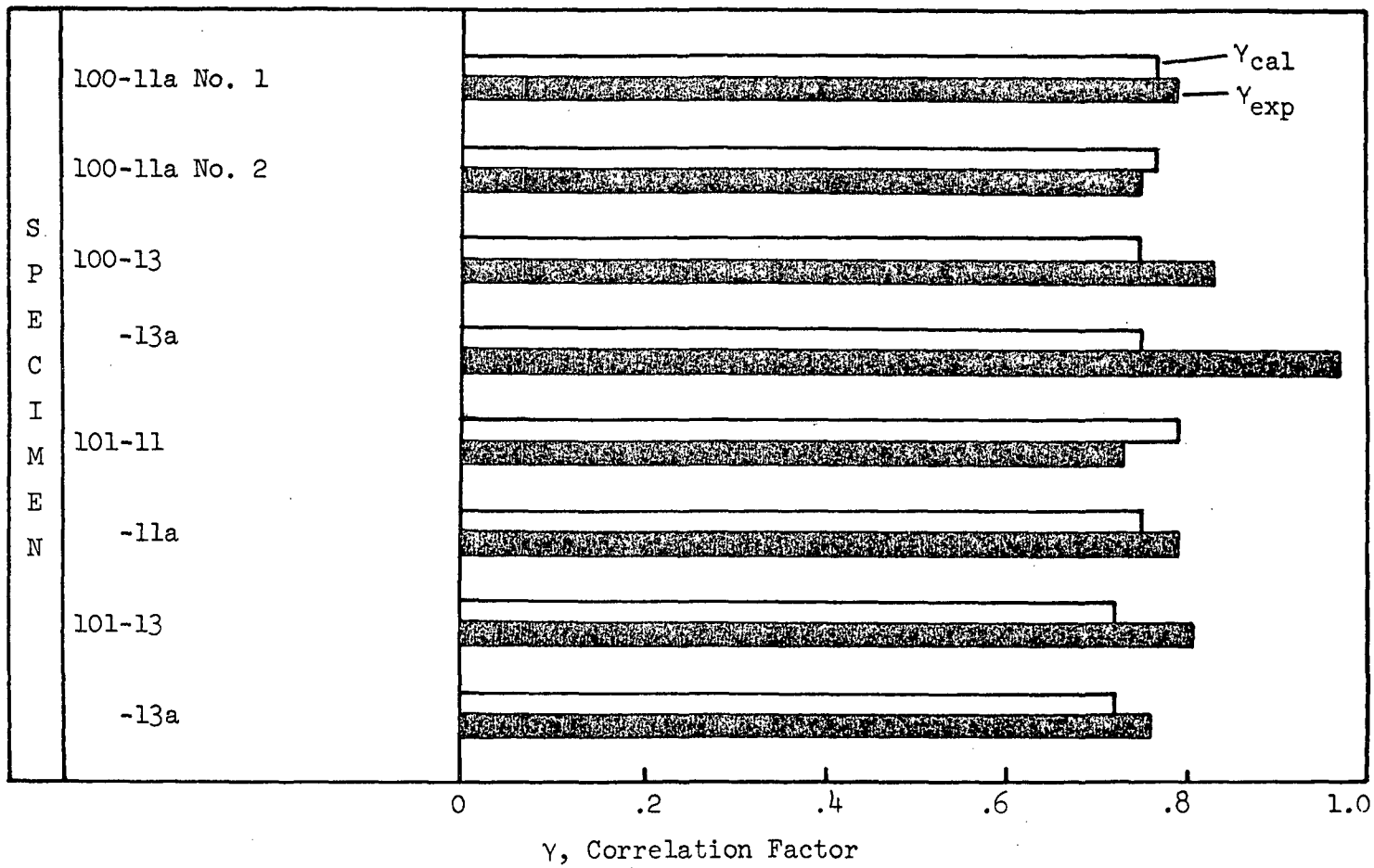

Figure 18. - Comparison of Calculated and Experimental Correlation Factors For Local Buckling Test Specimens